ORGANOMETALLICS

pubs.acs.org/Organometallics Article

Selective, Base-Free Hydrogenation of Aldehydes Catalyzed by Ir Complexes Based on Proton-Responsive Lutidine-Derived CNP Ligands

Práxedes Sánchez, Martín Hernández-Juárez, Nuria Rendón,* Joaquín López-Serrano, Eleuterio Álvarez, Margarita Paneque, and Andrés Suárez*

Cite This: *Organometallics* 2021, 40, 1314–1327 Read Online

ACCESS | Metrics & More | Article Recommendations | Supporting Information

ABSTRACT: Metal catalysts based on ligands containing proton-responsive sites have found widespread applications in the hydrogenation of polar unsaturated substrates. In this contribution, Ir complexes incorporating lutidine-derived CNP (C = N-heterocyclic carbene, NHC; P = phosphine) pincer ligands with two non-equivalent Brønsted acid/base sites have been examined in the hydrogenation of aldehydes. To this end, Ir(CNP)H_2Cl complexes were synthesized in two steps from the CNP ligand precursors and Ir(acac)(COD). These derivatives react with an excess of NaH to yield the trihydride derivatives Ir(CNP)H_3, which were assessed as catalyst precursors in the hydrogenation of a series of aldehydes. The catalytic reactions were performed using commercial-grade substrates under neutral, mild conditions (0.1 mol % Ir-CNP; 4 bar H_2, room temperature) with high conversions and selectivities for the reduction of the carbonyl function in the presence of other readily reducible groups such as C═C, nitro, and halogens. Reaction of an Ir(CNP)H_2Cl complex with base in the presence of an aromatic aldehyde produces the reversible formation of alkoxide Ir complexes in which the aldehyde is bound to the deprotonated pincer framework (CNP*) through the CH-NHC arm of the ligand. These species, along with a carboxylate complex resulting from the Ir mediated oxidation of the aldehyde by water, is observed in the reaction of Ir(CNP)H_3 with benzaldehyde. Finally, investigation of the mechanism of the hydrogenation of aldehydes has been carried out by means of DFT calculations considering the involvement of each arm of the Ir-CNP/CNP* derivatives. Calculations support a mechanism in which the catalyst switches its metal–ligand cooperation sites to follow the lowest energy pathway for each step of the catalytic cycle.

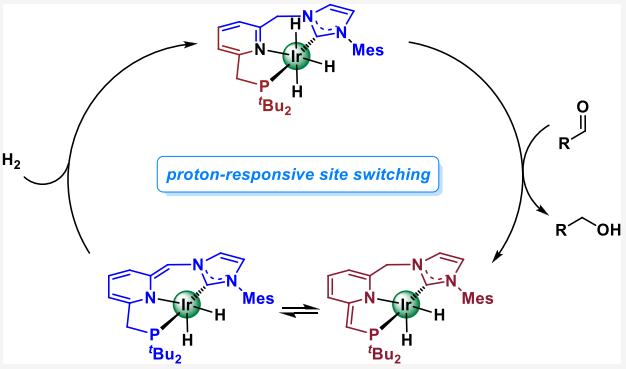

INTRODUCTION

Metal–ligand cooperation is a valuable concept for the design of novel catalysts for the development of sustainable, atom-economical catalytic hydrogenation and dehydrogenation reactions of polar substrates.[1] A prominent class of metal–ligand complexes containing Brønsted acid/base functionalities are those based on lutidine-derived PNX (P = phosphine, X = phosphine or a hemilabile N-donor) pincer ligands (Figure 1).[2] In these systems, the acidic $-CH_2-$ methylene arms can participate in reversible proton transfer processes leading to deprotonated metal species that are capable to activate H–Y (Y = H, heteroatom) bonds. An interesting modification of the PNX ligands resides in the substitution of the P-donors by N-heterocyclic carbenes (NHCs) of similar electron-donor strength (Figure 1).[3−5] Metal complexes based on these CNX (C = NHC, X = NHC or N-donor) ligands are also readily deprotonated at the methylene linkers and can participate in ligand-assisted processes. Moreover, this modification offers larger flexibility to the ligand due to the

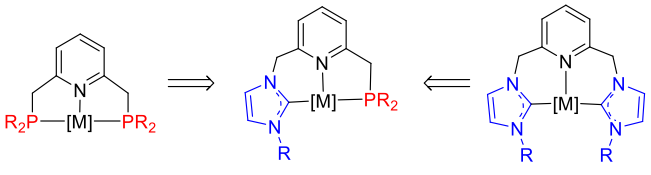

Figure 1. General structures of metal complexes with lutidine-derived PNP, CNC, and CNP ligands.

Received: February 24, 2021
Published: April 22, 2021

formation of 6-membered chelates upon coordination of the larger Py−CH_2−NHC linkage in comparison to the 5-membered rings provided by the PNX pincers. This higher flexibility has been shown in Ru−CNC* (* denotes a deprotonated lutidine-derived pincer) complexes to provide enhanced reactivities toward the ligand-assisted activation of H_2 and the binding of CO_2 to the deprotonated metal−ligand framework in comparison to analogous Ru−PNP* systems.[3]

A further approach to the development of improved catalytic systems that has been limitedly explored consists of the use of ligands incorporating two different Brønsted acid/base sites.[6] The underlying idea of this strategy is that the catalyst can switch its metal−ligand cooperation mode to choose the lowest energetically accessible pathway for each step of the catalytic cycle. Thus, metal complexes based on lutidine-derived ligands containing secondary amines as flanking donors have provided efficient catalysts in a variety of (de)hydrogenations of polar substrates.[7−9] Since these derivatives contain two acidic functionalities, they might exhibit metal−ligand cooperation based on both pyridine aromatization/dearomatization and amine-metal/amido-metal interconversion.[10] Another of such potentially dual-mode systems are metal complexes incorporating ligands based on a 2-hydroxypyridine fragment and a picoline arm.[11] However, in all the above-mentioned systems the large difference in basicity between both proton-responsive sites impedes changes in the metal−ligand cooperation modes, and the reactions proceed predominantly via a single form of metal−ligand cooperation (i.e., amine/amide interconversion).[12]

Recent research from our group has focused on the study of nonsymmetric lutidine-derived pincer ligands, i.e., having two inequivalent flanking donor groups,[13] particularly of the CNP class (Figure 1).[14−16] The presence of two significantly different strong σ-donors in the CNP pincer, such as a phosphine and a NHC, allows a larger electronic and steric diversity of the ligands, and facilitates a direct comparison of the relative acid/base reactivities of the NHC- and phosphine-bound methylene arms.

Herein, we report the synthesis of Ir complexes incorporating new CNP ligands having di-*tert*-butylphosphino side arms and their application to the chemoselective hydrogenation of commercial-grade aldehydes under neutral conditions. Aldehyde hydrogenation represents an environmentally friendly alternative to the use of alumino- and borohydrides commonly used in organic synthesis laboratories and industrial settings for the reduction of carbonyl groups.[17] Although hydrogenation of carbonyl derivatives, particularly ketones, is usually regarded as a well-developed technology, relatively few examples of catalytic systems have been described for the hydrogenation of aldehydes to primary alcohols,[18,19] most of them requiring previous extensive substrate purification and the use of a base as a catalyst activator, which is an important limitation to the reaction scope due to the sensitivity of aldehydes to basic conditions. Finally, experimental and theoretical mechanistic studies with the Ir-CNP complexes indicate that different acid/base sites of the CNP ligands are involved in the individual steps of the catalytic cycle.

RESULTS AND DISCUSSION

Ligand Synthesis. Alkylation of di-*tert*-butylphosphine with the imidazolium salt **1a** in CH_2Cl_2, followed by deprotonation of the resulting phosphonium salt **2a·HCl** after treatment with phenethyldiethylamine ScavengePore resin provided the imidazolium salt **2a** (Scheme 1). The CNP ligand precursor **2a**, which produces a broad resonance at

Scheme 1. Synthesis of Ligand Precursors 2

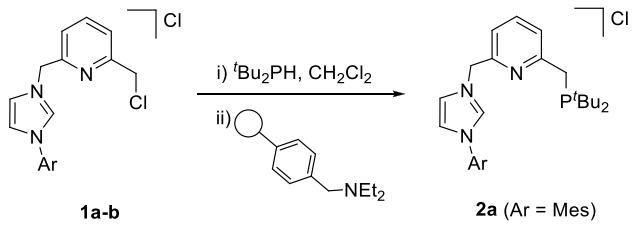

1a-b

2a (Ar = Mes)
2b (Ar = 3,5-Xyl)

37.1 ppm in the $^{31}P\{^1H\}$ NMR spectrum, was isolated with moderate purity (65−77% as determined by NMR), although it was employed without further purification for the synthesis of Ir-CNP complexes. An analogous procedure was used for the preparation of the ligand precursor **2b**.

Synthesis of Iridium Complexes. The preparation of Ir complexes containing the CNP ligands was initially assayed by the reaction of the imidazolium salt **2a** with Ir(acac)(COD).[14] This procedure led to the formation of the fully characterized complex **3** (Scheme 2). In the ^1H NMR spectrum, this derivative exhibits a doublet signal in the hydride region at −24.5 ppm ($^2J_{HP}$ = 17 Hz), and only two resonances (integrating for 3H each) in the region expected for the methyl substituents of the mesityl group (2.35 and 2.25 ppm). Moreover, two other resonances integrating for 1H are observed at 3.95 (d, $^2J_{HH}$ = 11.3 Hz) and 2.91 ppm (dd, $^2J_{HH}$ = 11.2 Hz, $^3J_{HP}$ = 9.1 Hz) that exhibit cross-peaks signals in the $^1H-^{13}C$ HSQC experiment with a carbon broad resonance appearing at δ_C −9.6 ppm, indicative of the presence of an Ir−C bond. Overall, these data points to the metalation of one of the CH_3 groups of the mesityl fragment,[20] as confirmed by a single-crystal X-ray diffraction analysis of the complex (Figure 2). Derivative **3** possesses, in the solid state, a slightly distorted octahedral geometry with the metalated CNP ligand adopting a planar coordination with C(1)−Ir(1)−P(1) and C(10)−Ir(1)−N(3) angles of 166.8° and 172.8°, respectively. Moreover, the existence of a hydrogen bond between the chloride ligand and the axial hydrogen of the CH_2N arm is evident from the H···Cl distance of 2.6 Å, which is shorter than the sum of van der Waals radii of H and Cl (2.9−3.0 Å).[21] This interaction is also manifested in the significant deshielding of the doublet resonance corresponding to the axial C*H*HN hydrogen in the ^1H NMR spectrum (δ_H 7.07 ppm, $^2J_{HH}$ = 14.6 Hz).

Overnight exposure to H_2 (4 bar) of a solution heated to 65 °C of **3** in CH_2Cl_2 produced the formation of the chlorodihydride complex **4a**, which was isolated quantitatively as a yellow solid (Scheme 2). The hydride region of the ^1H NMR spectrum of **4a** shows two doublets of doublets at −20.36 ($^2J_{HP}$ = 14.4 Hz, $^2J_{HH}$ = 6.5 Hz) and −24.89 ppm ($^2J_{HP}$ = 17.2 Hz, $^2J_{HH}$ = 6.5 Hz) attributable to the IrH *trans* and *cis* to the pyridine fragment, respectively. In the $^{13}C\{^1H\}$ NMR experiment, the C-2 NHC was observed as a doublet resonance appearing at 173.2 ppm with a large J_{CP} coupling constant of 115 Hz, suggesting *trans* coordination of the NHC and phosphine fragments of the pincer. Pressurization of a solution of **4a** in CD_2Cl_2 at room temperature with deuterium gas (3 bar) produced after 5 h the complete H/D scrambling of the hydrido ligands. However, deuterium incorporation at

https://doi.org/10.1021/acs.organomet.1c00109
Organometallics 2021, 40, 1314−1327

Scheme 2. Synthesis of Complexes 3, 4a, and 6a

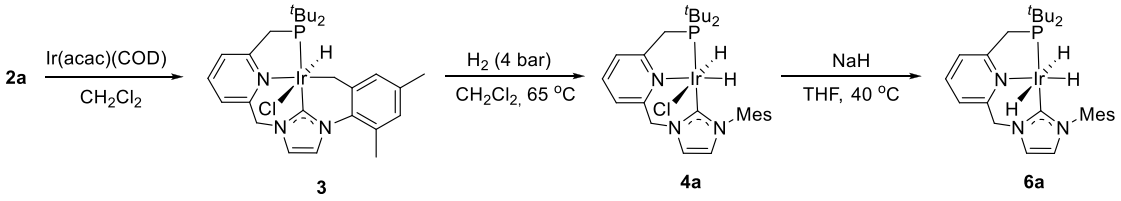

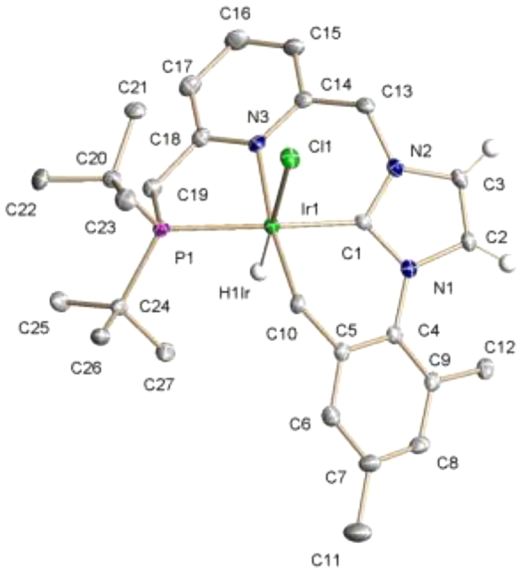

Figure 2. ORTEP drawing at 30% ellipsoid probability of complex **3**. Most hydrogen atoms have been omitted for clarity. Selected bond lengths [Å] and angles [°]: Ir(1)−C(1) 1.980(5), Ir(1)−N(3) 2.139(4), Ir(1)−P(1) 2.32271(12), Ir(1)−C(10) 2.085(5), Ir(1)−Cl(1) 2.5616(11), C(1)−Ir(1)−P(1) 166.79(16), C(1)−Ir(1)−C(10) 83.44(18), C(10)−Ir(1)−N(3) 172.79(16), C(1)−Ir(1)−N(3) 89.47(17), P(1)−Ir(1)−N(3) 82.24(11), C(10)−Ir(1)−P(1) 104.97(13).

the methylene arms of the pincer was not observed even after prolonged heating of the sample to 50 °C (72 h).

On the other hand, reaction of the xylyl substituted salt **2b** with Ir(acac)(COD) in CH_2Cl_2 followed by exposure to H_2 (4 bar) at room temperature produced the expected dihydride complex **4b** (Scheme 3).[14] Interestingly, formation of **4b** was accompanied of the hydrogenation of the imidazolylidene ligand fragment yielding an inseparable mixture of **4b** and **5** formed in an 8:2 ratio. The addition of dihydrogen to the C═C double bond of the imidazolylidene moiety was readily

Scheme 3. Synthesis of Complexes 4b, 5, 6b, and 7

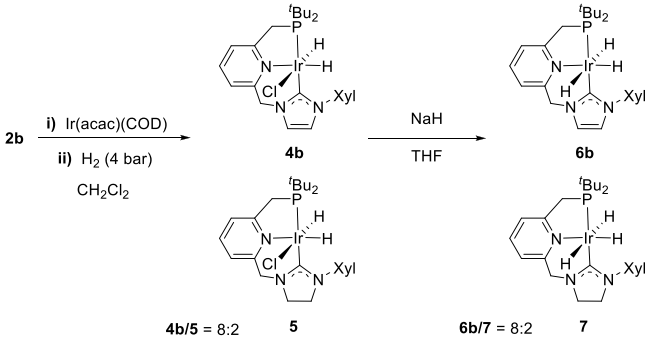

deduced from the observation of new multiplet signals at 3.91 (integrating to 2H) and 4.05 and 4.30 ppm (1H each) in the ^{1}H NMR spectrum assignable to the $-CH_2CH_2-$ linkage of the imidazolidinylidene donor. The hydride ligands of **5** produce two doublet of doublets appearing at −20.41 ($^2J_{HP}$ = 14.5 Hz, $^2J_{HH}$ = 5.9 Hz) and −24.40 ppm ($^2J_{HP}$ = 17.8 Hz, $^2J_{HH}$ = 5.9 Hz) that correspond to the equatorial and axial hydrido ligands, respectively. Hydrogenation of an imidazolylidene ligand has previously been observed in a related system.[15]

Finally, in order to obtain trihydride Ir-CNP complexes that may serve as hydrogenation catalysts, complex **4a** was treated with an excess of NaH in THF leading to the formation of **6a**, which is stable in the solid state under atmospheric conditions for extended periods of time, albeit readily reacts with chlorinated solvents leading to the regeneration of **4a** (Scheme 2). The apical hydrido ligands of **6a** produce in the ^{1}H NMR spectrum a doublet of doublets at −10.14 ppm ($^2J_{HP}$ = 15.6 Hz, $^2J_{HH}$ = 5.4 Hz), whereas a doublet of triplets appearing at −20.03 ppm ($^2J_{HP}$ = 13.8 Hz, $^2J_{HH}$ = 5.4 Hz) can be ascribed to the meridional IrH hydrogen. Similarly, reaction of the mixture of **4b** and **5** with NaH produced the formation of an 8:2 mixture of **6b** and **7** (Scheme 3).

Upon exposure of a toluene-d_8 solution of the trihydride derivative **6a** to D_2 (5 bar, r.t., 20 h), the hydrido ligands and the methylene bridges underwent partial H/D exchange, suggestive of the reversible exchange of free D_2 with a η^2-H_2 ligand resulting from the intramolecular protonation of Ir−H hydrogens by protons of both the P-CH_2 and NHC-CH_2 methylene fragments (Scheme 4).[22] This observation can be regarded as an indirect evidence of ligand-assisted H−H activation.

Hydrogenation of Aldehydes. In order to assess the catalytic potential of the trihydride Ir−CNP complexes, their performance in the chemoselective hydrogenation of *commercial-grade* aldehydes was studied (Table 1). Using a catalyst loading of 0.5 mol %, complex **6a** smoothly catalyzed the hydrogenation of benzaldehyde under 4 bar of H_2 at 25 °C in 2-methyltetrahydrofuran[23] with a conversion of 70% (entry 1). The catalysts mixture **6b**/**7** was also examined under the same conditions providing a similar catalytic activity (entry 2). By using higher concentrations of substrate and lower catalyst loadings (0.1 mol %) of **6a**, benzaldehyde was hydrogenated with 96% conversion (entry 3). Under the latter reaction conditions, a series of substituted aromatic aldehydes was tested in order to determine the chemoselectivity and functional group tolerance of the catalytic system. The hydrogenation of substrates bearing halogen substituents was carried out with high conversions, and no hydrogenolysis of the C−X bond was detected (entries 4 and 5). Similarly, 4-nitrobenzaldehyde was selectivity hydrogenated to the corresponding alcohol without observable reduction of the nitro group (entry 6), whereas trifluoromethyl substituted benzaldehyde was reduced with 76% conversion (entry 7).

https://doi.org/10.1021/acs.organomet.1c00109
Organometallics 2021, 40, 1314−1327

Scheme 4. Deuteration of 6a with D_2 and Proposed Mechanism for the Observed H/D Exchanges

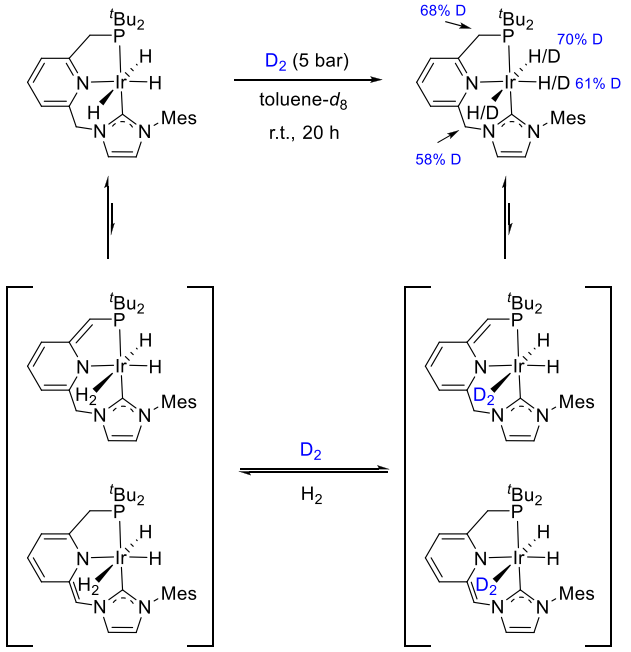

Moreover, hydrogenation of vanillin was accomplished with complete conversion (entry 8). Finally, the hydrogenation of alkyl substituted aldehydes was examined using complex **6a**. Hexanal, 2-methylpentanal, and cyclohexanecarboxaldehyde were hydrogenated with conversions higher than 91% (entries 9−11).

Since the chemoselective reduction of aldehydes containing a C═C bond is a relevant process in the industrial production of fine chemicals and pharmaceutical compounds,[24] the hydrogenation of a series of C═C unsaturated aldehydes was next examined with **6a** (Table 2). The reduction of *trans*-cinnamaldehyde, containing a conjugated C═C double bond, to the corresponding alcohol was performed with high conversion and elevated selectivity using the previously optimized reaction conditions (entry 1). Instead, the hydrogenation of *trans*-2-hexen-1-al required an increase of the catalyst loading to 0.5 mol % to obtain an admissible conversion (entry 2). The hydrogenation of citronellal took place with complete conversion and a selectivity of 99% (entry 3), whereas cis/trans isomerization of the C═C double bond was not observed in the reaction of citral, a 1:0.6 mixture of geranial and neral (entry 4).

Mechanistic Studies. Initially, the reactivity of the Ir complex **4a** with base in the presence of aldehyde was investigated to get further insight into the acid−base properties of the methylene bridges of the lutidine-derived CNP ligand.[14−16] Addition of potassium bis(trimethylsilyl)amide (KHMDS) or *t*BuOK (1.1 equiv) to a solution of **4a** and benzaldehyde (3 equiv) in THF-d_8 brought about the formation of two diastereomeric dihydride species, **8a**$^{\mathbf{M}}$ and **8a**$^{\mathbf{m}}$, in a 9.4:0.6 ratio (Scheme 5). These derivatives are formally derived from the addition of the aldehyde to the Ir-CNP* framework deprotonated at the NHC-bound arm. Similarly, complex **4a** in the presence of KHMDS (1.1 equiv) reacted with *p*-bromobenzaldehyde in THF-d_8, yielding the isomers **8b**$^{\mathbf{M}}$ and **8b**$^{\mathbf{m}}$, also formed in a 9.4:0.6 ratio. Complexes based on deprotonated PNP* and CNC* lutidine-derived pincer ligands have been shown to exhibit Frustrated Lewis Pair-type reactivity toward electrophiles such as CO_2, carbonyl compounds, nitriles, and imines.[3,5,25]

Table 1. Hydrogenation of Aldehydes Catalyzed by Ir-CNP Complexes[a]

Entry	Aldehyde	Ir-CNP	Conv. (%)
1[b]	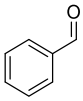	6a	72
2[b]		6b/7	70
3		6a	96
4	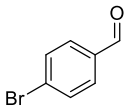	6a	>99
5	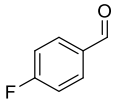	6a	96
6	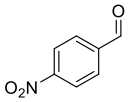	6a	>99
7	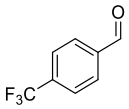	6a	76
8	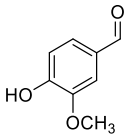	6a	>99
9	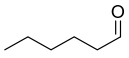	6a	92
10	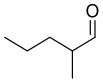	6a	98
11		6a	91

[a]Reaction conditions, unless otherwise noted: 4 bar of H_2, 2-methyltetrahydrofuran, 0.1 mol % Ir-CNP, 25 °C, 24 h. [S] = 2.0 M. Conversion was determined by ^{1}H NMR spectroscopy using mesitylene as internal standard. [b]0.5 mol % Ir-CNP, [S] = 0.3 M, 6 h.

In the ^{1}H NMR spectrum, the hydrido ligands of the major complex **8a**$^{\mathbf{M}}$ produce two doublets of doublets at −19.39 ($^2J_{HP}$ = 14.2 Hz, $^2J_{HH}$ = 7.8 Hz) and −24.33 ($^2J_{HP}$ = 18.2 Hz, $^2J_{HH}$ = 7.8 Hz) ppm, whereas **8a**$^{\mathbf{m}}$ also shows two doublet of doublets for the IrH hydrogens appearing at −20.06 ($^2J_{HP}$ = 13.7 Hz, $^2J_{HH}$ = 7.4 Hz) and −24.11 ($^2J_{HP}$ = 18.5 Hz, $^2J_{HH}$ = 7.4 Hz) ppm. The presence of an intense cross-peak signal in the ^{1}H−^{1}H NOESY spectrum between one of the resonances corresponding to the CH_2P arm (δ 2.95 ppm) and one of the hydrido ligands (δ −24.33 ppm) of the major isomer **8a**$^{\mathbf{M}}$ allows to assign the resonance appearing at higher field in the hydride region to the apical hydride. Moreover, the formation of the new carbon−carbon bond is deduced from the appearance of a singlet at 4.90 ppm corresponding to the alkoxide −C(Ph)H−O−Ir fragment, which exhibits an intense cross-peak with the singlet resonance due to the CHN moiety (δ_H 5.64 ppm) in the ^{1}H−^{1}H NOESY spectrum. The former

https://doi.org/10.1021/acs.organomet.1c00109
Organometallics 2021, 40, 1314−1327

Table 2. Hydrogenation of Unsaturated Aldehydes Catalyzed by Complex 6a[a]

Entry	Aldehyde	Conv. (%)	Ratio unsaturated/saturated alcohol (%)
1	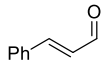	>99	99:1
2[b]	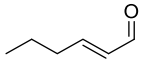	84	88:12
3	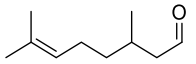	>99	99:1
4[c]	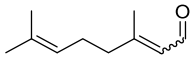	>99	96:4

[a]Reaction conditions, unless otherwise noted: 4 bar of H_2, 2-methyltetrahydrofuran, 0.1 mol % **6a**, 25 °C, 24 h. [S] = 2.0 M. Conversion was determined by ^{1}H NMR spectroscopy using mesitylene as internal standard. [b]0.5 mol % **6a**, [S] = 1.0 M. [c]Geranial/neral ratio = 1:0.6.

Scheme 5. Formation of Complexes 8

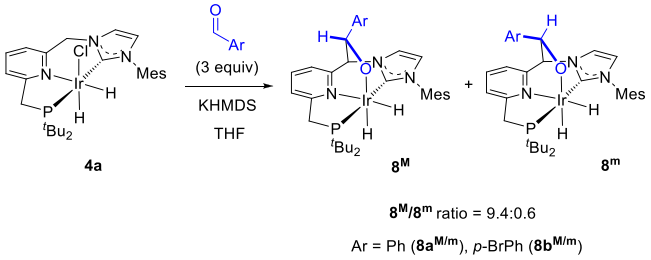

signal is significantly shifted upfield with respect to the chemical shift of the carbonyl hydrogen of the free aldehyde (δ_H 10.0 ppm), as expected from a change in the sp^2 hybridization of the carbonyl carbon to sp^3. Further confirmation of the assignment of this signal was obtained from the existence of an exchange cross-peak in the ^{1}H−^{1}H EXSY spectrum with the resonance of the carbonyl proton of free benzaldehyde, also suggesting the reversible exchange between coordinated and free benzaldehyde.

The relative stabilities of **8a**^{M} and **8a**^{m} were studied using DFT calculations (B3LYP-D3, 6-31g(d,p)/SDD). The product of the *exo* coordination of benzaldehyde to the deprotonated Ir-CNP* framework was found to be 0.9 kcal mol^{-1} more stable than the result of binding of the aldehyde through the opposite face (*endo*), indicating that the major complex **8**^{M} should coordinate the aldehyde *exo*, whereas **8**^{m} corresponds to the *endo* coordination of the carbonyl compound. Further confirmation of this assignment was obtained from the observation of a strong cross-peak due to the resonances of the CHO−Ir moiety and one of the *t*Bu groups of **8a**^{M} in the ^{1}H−^{1}H NOESY spectrum. Moreover, calculations also showed that adducts resulting from the coordination of benzaldehyde to the Ir-CNP* framework deprotonated at the phosphine arm are 14.0 (*exo* isomer) and 8.7 kcal/mol (*endo* isomer) higher in energy with respect to **8a**^{M}. The lower stability of these isomers can be attributed to the higher steric hindrance caused by the bulky di(*tert*-butyl)phosphino donor fragment.

The structure of complex **8b**^{M} in the solid state was corroborated by the X-ray diffraction analysis of a single crystal (Figure 3). This is composed by a distorted octahedral Ir(III)

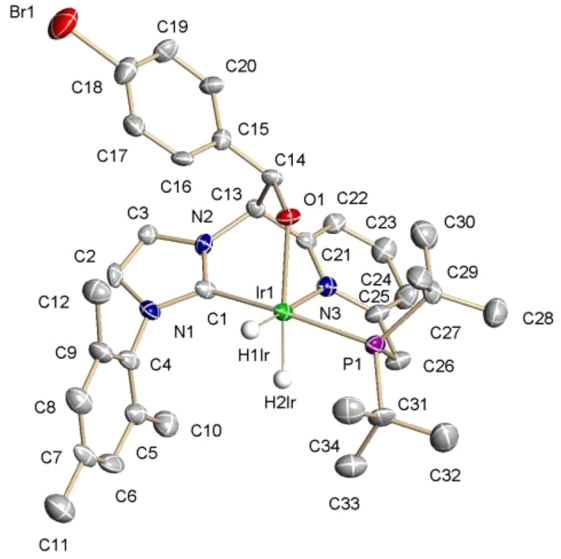

Figure 3. ORTEP drawing at 30% ellipsoid probability of complex **8b**^{M}. Most hydrogen atoms have been omitted for clarity. Selected bond lengths [Å] and angles [°]: Ir(1)−C(1) 2.005(11), Ir(1)−N(3) 2.142(10), Ir(1)−O(1) 2.219(7), Ir(1)−P(1) 2.283(3), C(13)−C(14) 1.591(16), C(14)−O(1) 1.369(13), C(1)−Ir(1)−P(1) 168.5(3), C(1)−Ir(1)−O(1) 82.6(4), O(1)−Ir(1)−N(3) 82.4(3), C(1)−Ir(1)−N(3) 90.2(4), P(1)−Ir(1)−N(3) 81.2(3).

complex with the pincer adopting a meridional coordination and the hydrido ligands in mutually *cis* positions. The C−C bond distance between the carbonyl carbon and the CH arm (C14−C13 = 1.591 Å) is characteristic for a C−C single bond, whereas the C14−O1 of 1.369 Å exhibits a typical value for single C−O binding. The Ir1−O1 bond (2.219 Å) is in the range of other Ir-OR bond distances.[26]

Addition at room temperature of benzaldehyde(1.8 equiv) to a THF-d_8 solution of complexes **8b** gave within minutes a mixture of **8a**^{M} and **8b**^{M}, a further indication for the reversibility of the formation of the C−C and O−Ir bonds. Relative thermodynamic stabilities of complexes **8a**^{M} and **8b**^{M} were determined from the observed equilibrium **8a**^{M} + *p*-bromobenzaldehyde ⇌ **8b**^{M} + benzaldehyde by using ^{1}H NMR spectroscopy. From the calculated $^{298}K_{eq}$ = 7.2, a stability order of the adducts **8b**^{M} > **8a**^{M} was estimated, as expected from the higher electrophilicity of the carbonyl carbon of *p*-bromobenzaldehyde.

Since aldehyde coordination to the Ir-CNP* framework deprotonated at the NHC-arm (**A**^{NHC}) was found to be reversible, the study of the isomerization of **A**^{NHC} to the Ir-CNP* species deprotonated at the P-bound bridge (**A**^{P}) was deemed interesting. To this end, a solution of the in situ generated complex **8a** was treated with MeOD-d_3 producing the deuteration of the CH-NHC methyne and CH_2−P methylene bridges (Scheme 6). As previously shown above with the deuteration of **6a** with D_2, this result can be regarded as an indirect proof of the feasibility of the interconversion between the two tautomeric forms of Ir(CNP*)H_2, **A**^{NHC} and **A**^{P} (see below).[16]

Next, aiming to elucidate the species participating in the hydrogenation of aldehydes catalyzed by Ir-CNP complexes,

https://doi.org/10.1021/acs.organomet.1c00109
Organometallics 2021, 40, 1314−1327

Scheme 6. Deuteration of 8a with MeOD-d_3

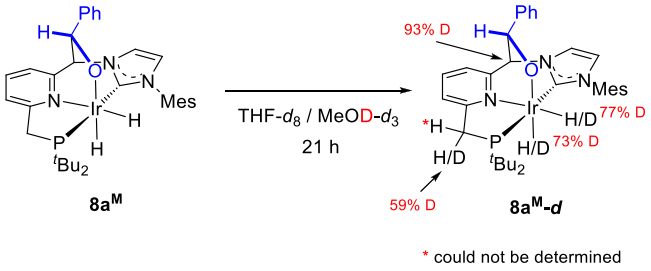

the reaction of the trihydride complex **6a** with benzaldehyde (4.0 equiv) in THF-d_8 was examined by NMR spectroscopy (Scheme 7). In the ^{1}H NMR spectrum, signals attributable to

Scheme 7. Reaction of 6a with Benzaldehyde

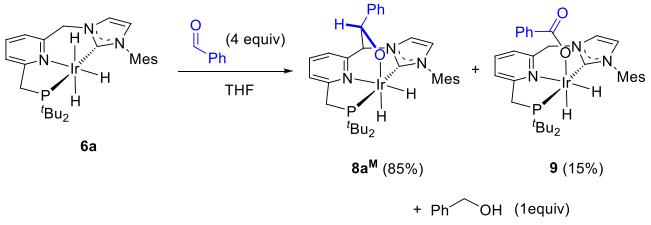

the formation of **8a^M** (85%), a new species **9** (15%), and benzyl alcohol (1 equiv with respect to **8a^M**) were observed. Complex **9** was isolated from the reaction mixture and characterized by NMR spectroscopy and X-ray diffraction techniques as a η^1-carboxylate Ir(CNP)(PhCO$_2$)H$_2$ complex. In the solid state, the structure of **9** shows an Ir center in an octahedral geometry in which the pincer ligand is meridionally coordinated, and the apical coordination sites are occupied by one hydrido and the carboxylate ligands (Figure 4). The Ir(1)−O(1) bond length (2.225(2) Å) lies in the range of other Ir−O distances in complexes with carboxylate ligands coordinated *trans* to H.[26] Moreover, the carboxylate group shows little change with respect to the free benzoate, as reflected in the O(1)−C(28)−O(2) angle of 127.7(4)°, and in the similar values of both oxygen−carbon bond distances (O(1)−C(28) = 1.262(4) Å; O(2)−C(28) = 1.242(5) Å).

The ^{1}H NMR spectrum of **9** in CD_2Cl_2 shows, in the hydride region, two doublets of doublets at −19.91 ($^2J_{HP}$ = 14.4 Hz, $^2J_{HH}$ = 6.7 Hz) and −26.85 ($^2J_{HP}$ = 17.1 Hz, $^2J_{HH}$ = 6.7 Hz) ppm, corresponding to the IrH hydrogens *trans* and *cis* to the pyridine fragment, respectively. Relevant signals of **9** in the ^{13}C{^{1}H} NMR spectrum include a doublet at δ 174.7 ppm (J_{CP} = 116 Hz) produced by the C-2 NHC carbon, and a resonance at δ 171.0 ppm due to the carboxylic carbon. In the ^{1}H−^{1}H exchange spectroscopy (EXSY) spectrum of **9** registered at 25 °C intense exchange cross-peaks are observed between the signals corresponding to the hydride ligands, as well as between the resonances of the diastereotopic CH$_2$−P and CH$_2$−NHC hydrogens. This observation points to the existence of an exchange process that should involve the reversible decoordination of the benzoate ligand facilitated by the large trans influence of the apical hydride, or the reversible elimination of benzoic acid after intramolecular protonation of the carboxylate ligand by the methylene linkers of the pincer (see the Supporting Information).

As formation of complex **9** was thought to take place by an Ir promoted aldehyde oxidation by adventitious water present

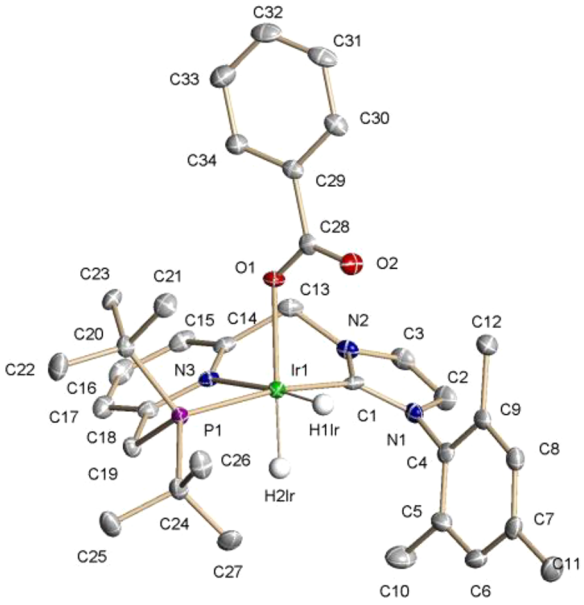

Figure 4. ORTEP drawing at 30% ellipsoid probability of complex **9**. Most hydrogen atoms have been omitted for clarity. Selected bond lengths [Å] and angles [°]: Ir(1)−C(1) 2.016(4), Ir(1)−N(3) 2.173(3), Ir(1)−O(1) 2.225(2), Ir(1)−P(1) 2.2772(9), C(28)−O(1) 1.262(4), C(1)−Ir(1)−P(1) 165.83(10), C(1)−Ir(1)−O(1) 91.19(12), O(1)−Ir(1)−N(3) 88.32(10), C(1)−Ir(1)−N(3) 88.42(13), P(1)−Ir(1)−N(3) 82.04(8).

in the commercial aldehyde,[27] an independent synthesis of this derivative was sought. Addition of deionized H$_2$O to a heated THF solution of **8a^M**/**8a^m** (formed in situ from **4a**, KHMDS and a 3-fold excess of benzaldehyde) produced the initially dark red solution to turn gradually to yellow, bringing about the clean formation of **9** (Scheme 8). However, in order to rule

Scheme 8. Synthesis of Complex 9

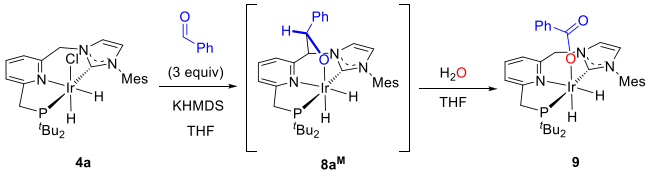

out the role of adventitious atmospheric oxygen in the formation of **9**,[28] a THF solution of complex **8a^M** was heated under air leading to a complex reaction mixture. This suggests that O_2 is not the oxygen source in the reaction. Nonetheless, to further demonstrate that water is the oxygen donor, synthesis of ^{18}O-labeled **9** was carried out using H$_2$^{18}O. The high resolution MS spectrum (ESI ionization, positive mode) of the complex exhibits signals at m/z = 750.2790, 752.2836, and 754.2880, which according to their isotopic distribution can be assigned to [Ir(CNP)H(PhC^{16}O$_2$)]$^+$, [Ir(CNP)H-(PhC^{16}O^{18}O)]$^+$, and [Ir(CNP)H(PhC^{18}O$_2$)]$^+$, respectively. Similarly, in the negative mode of the HRMS spectrum, signals at m/z = 121.0295, 123.0337, and 125.0380, corresponding to [PhC^{16}O$_2$]$^+$, [PhC^{16}O^{18}O]$^+$, and [PhC^{18}O$_2$]$^+$, respectively, are obtained. These analyses confirmed ^{18}O incorporation into the final product, and demonstrate that water is the oxygen source in the synthesis of the carboxylate complex **9**.

Finally, the reaction of a mixture of complexes **8a^M** and **9**, obtained from the reaction of **6a** with benzaldehyde (4 equiv),

https://doi.org/10.1021/acs.organomet.1c00109
Organometallics 2021, 40, 1314−1327

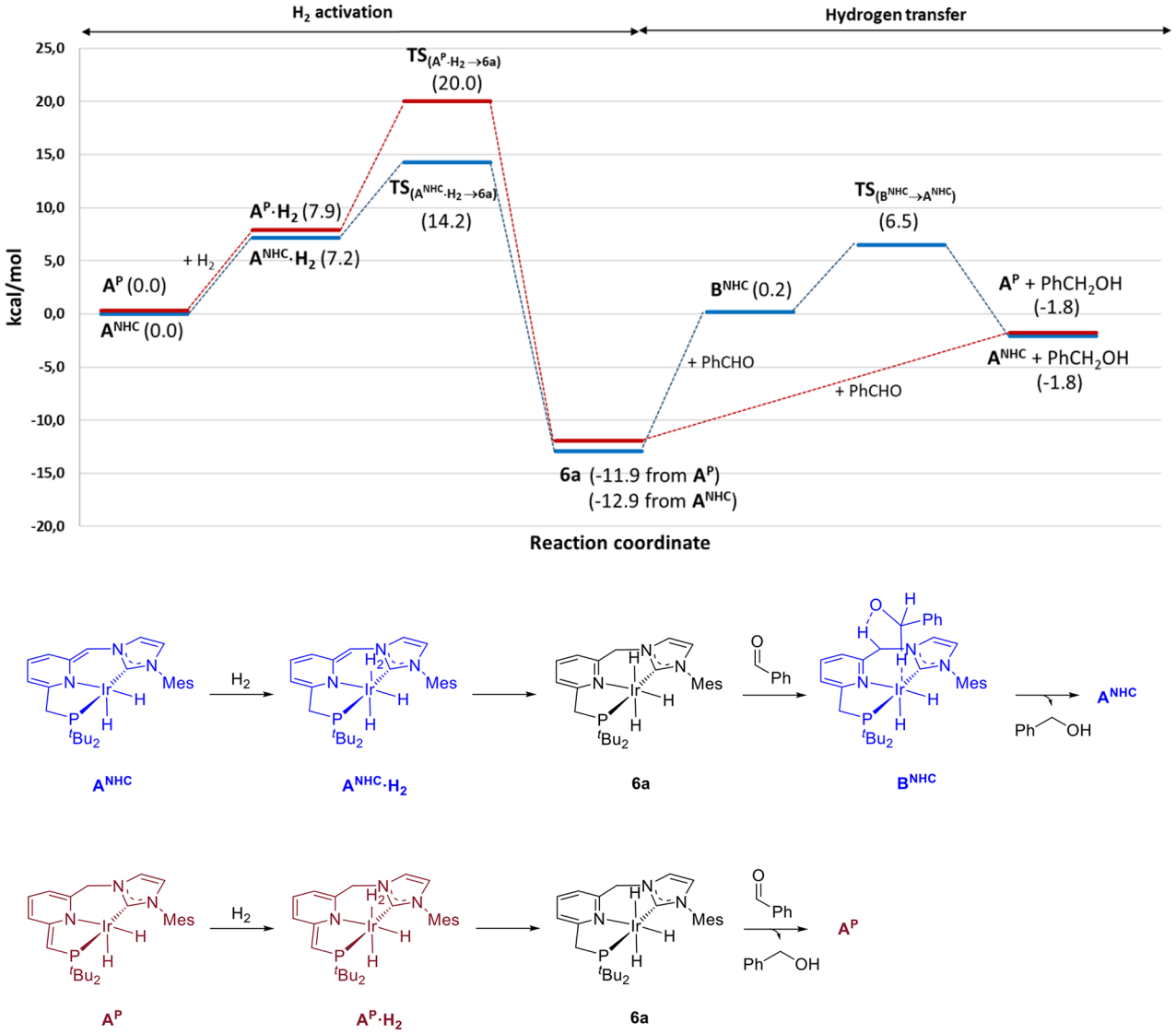

Figure 5. DFT calculated free energy (ΔG in THF, kcal/mol) profile and reaction steps of the hydrogenation of benzaldehyde catalyzed by **6a**. Note that the origin of energies is $\mathbf{A}^{\mathbf{P}}$ + H_2 + benzaldehyde (red line) and $\mathbf{A}^{\mathbf{NHC}}$ + H_2 + benzaldehyde (blue line).

with H_2 (2 bar) was followed up by ^{1}H and ^{31}P{^{1}H} NMR spectroscopy. Hydrogenation of benzaldehyde was ensued, being adduct $\mathbf{8a}^{\mathbf{M}}$ and carboxylate **9** the major observable Ir species until complete conversion of the aldehyde took place and complex $\mathbf{8a}^{\mathbf{M}}$ was transformed to the trihydride derivative **6a** (see Supporting Information). Moreover, a control experiment involving the hydrogenation of *p*-bromobenzaldehyde (room temperature, 3 bar of H_2, tetrahydrofuran, 4 h) catalyzed by **9** (1.0 mol %) demonstrated that the carboxylate complex is also a competent catalyst precursor.[19]

DFT Calculations. The assumption of an outer-sphere, ligand-assisted mechanism for the hydrogenation of aldehydes catalyzed by complexes **6** seems plausible on the basis of the experimental results discussed above, albeit different pathways involving the CH_2−P and CH_2−N methylene linkers of the pincer can be hypothesized. Therefore, we deemed it interesting to explore theoretically the mechanism of the hydrogenation of aldehydes by complexes **6** by the performance of DFT calculations (B3LYP-D3, 6-31g(d,p)/SDD). Initially, since complex $\mathbf{8a}^{\mathbf{M}}$ was experimentally determined to be a suitable catalyst precursor, the dissociation of benzaldehyde from $\mathbf{8a}^{\mathbf{M}}$ leading to the formation of intermediate $\mathbf{A}^{\mathbf{NHC}}$, which is deprotonated at the NHC-arm of the pincer, was examined. The formation of $\mathbf{8a}^{\mathbf{M}}$ was found to be exergonic by 11.0 kcal/mol. Moreover, in addition to $\mathbf{A}^{\mathbf{NHC}}$, the existence of the isomer $\mathbf{A}^{\mathbf{P}}$, deprotonated at the P-bridge of the pincer, can also be hypothesized.[16] This derivative was found to be 1.0 kcal/mol more stable than $\mathbf{A}^{\mathbf{NHC}}$.

Calculations of the catalytic cycle were commenced by considering the heterolytic H_2 cleavage from the η^2-H_2 adducts $\mathbf{A}^{\mathbf{P}}$·$\mathbf{H_2}$ and $\mathbf{A}^{\mathbf{NHC}}$·$\mathbf{H_2}$, which are 7.9 and 7.2 kcal/mol less stable than $\mathbf{A}^{\mathbf{P}}$ + H_2 and $\mathbf{A}^{\mathbf{NHC}}$ + H_2, respectively (Figure 5). This process takes place through concerted four-membered transition states ($\mathbf{TS}_{\mathbf{A(NHC)\rightarrow 6a}}$ and $\mathbf{TS}_{\mathbf{A(P)\rightarrow 6a}}$), having energy barriers ($\Delta G^{\ddagger}$) of 7.0 and 12.1 kcal/mol, respectively (Figure 6). The hydrogenation of $\mathbf{A}^{\mathbf{P}}$ and $\mathbf{A}^{\mathbf{NHC}}$ is energetically favorable, yielding **6a** with energy returns of 11.9 and 12.9 kcal/mol, respectively.

Next, ligand-assisted hydrogenation of benzaldehyde by **6a** was calculated to proceed with the participation of the CH_2−P arm of the pincer as the proton source to yield benzyl alcohol

https://doi.org/10.1021/acs.organomet.1c00109
Organometallics 2021, 40, 1314−1327

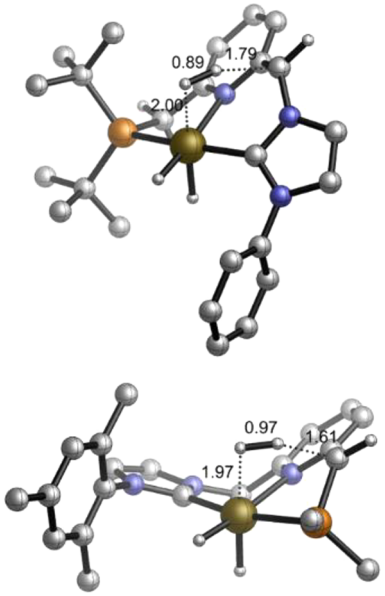

Figure 6. Views of the DFT-optimized geometries of the transition states $\mathbf{TS}_{\mathbf{A(NHC)\cdot H2\rightarrow 6a}}$ (top) and $\mathbf{TS}_{\mathbf{A(P)\cdot H2\rightarrow 6a}}$ (bottom). Methyl groups of the mesityl (top) and *t*-Bu (bottom) fragments have been omitted for clarity.

and regenerate the deprotonated complex $\mathbf{A}^{\mathbf{P}}$. This step is endergonic by 10.1 kcal/mol from **6a** (+ benzaldehyde), while the reverse step is barrierless, as indicated by relaxed potential energy (PES) scans (see the Supporting Information). Conversely, calculations have showed a stepwise hydrogen transfer when the CH_2−NHC arm of the Ir complex **6a** was the proton source. This process takes place through the initial formation of the less stable intermediate $\mathbf{B}^{\mathbf{NHC}}$ after hydride attack to the carbonyl carbon (in this case, a TS was located for the formation of $\mathbf{B}^{\mathbf{NHC}}$, and dissociation of the aldehyde to regenerate **6a** was shown to be almost barrierless). Subsequent proton abstraction from the CH_2−NHC bridge of the pincer yields benzyl alcohol and $\mathbf{A}^{\mathbf{NHC}}$. This step has a barrier of 6.3 kcal/mol, amounting the overall energy barrier from **6a** to 19.4 kcal/mol. The full hydrogen transfer from **6a** to the aldehyde to regenerate $\mathbf{A}^{\mathbf{NHC}}$ is endergonic by 11.1 kcal/mol. The observed differences in the hydrogen transfer to the aldehyde involving the methylene CH_2−P and CH_2−NHC arms of the catalyst can be ascribed to the slightly higher acidic character of the phosphine containing arm.

Overall, DFT calculations of the mechanism of the hydrogenation of aldehydes catalyzed by the Ir-CNP complex **6a** show that H_2 activation is easier for the deprotonated species $\mathbf{A}^{\mathbf{NHC}}$ than for $\mathbf{A}^{\mathbf{P}}$ ($\Delta\Delta G^{\ddagger}$ = 5.8 kcal/mol), whereas a more favorable process takes place when the methylene CH_2−P bridge of the catalyst is involved in the hydrogen transfer step. Although different mechanisms for the interconversion of $\mathbf{A}^{\mathbf{P}}$ and $\mathbf{A}^{\mathbf{NHC}}$ can be invoked, a potential pathway could involve proton transfer assisted by protic molecules (water or alcohol) (see the Supporting Information).[16,29] The likeliness of such a process has been indirectly evidenced by the observed deuteration of the CH-NHC methyne and CH_2−P methylene bridges of **8a** with MeOD-d_3 (see above).

CONCLUSIONS

We have demonstrated that lutidine-derived CNP iridium complexes, having two nonequivalent Brønsted acid/base sites, are efficient catalysts in the hydrogenation of commercial-grade aldehydes. The catalytic reactions are readily performed under neutral, mild (25 °C, 4 bar H_2) conditions using low catalyst loadings (0.1 mol %) with high selectivities toward the reduction of the carbonyl group in the presence of other reducible functions. Experimental and theoretical studies support that both CH_2−NHC and CH_2−P methylene bridges of the pincer can participate in ligand-assisted processes. However, while participation of the NHC-arm of the pincer is favored in the H_2 activation step of the catalytic cycle, hydrogen transfer to the aldehyde is easier when the process is assisted by the CH_2−P bridge. Since, according to experimental results, interconversion between the two deprotonated forms of the catalyst ($\mathbf{A}^{\mathbf{P}}$ and $\mathbf{A}^{\mathbf{NHC}}$) seems facile, the lowest energy pathway in the catalytic cycle involves a switch of the metal−ligand cooperation site. Due to the widespread use of metal complexes containing Brønsted acid/base functionalities in hydrogenation and dehydrogenation reactions, we think that the above-mentioned approach (i.e., use of two nonequivalent proton-responsive sites with similar acid/base properties) could be a fruitful approach to catalyst development.

EXPERIMENTAL SECTION

General Information. All reactions and manipulations were performed under nitrogen or argon atmosphere, either in a Braun Labmaster 100 glovebox or using standard Schlenk-type techniques. All solvents were dried and distilled under nitrogen, using the following desiccants: sodium-benzophenone-ketyl for diethyl ether (Et_2O), tetrahydrofuran (THF), and 2-methyltetrahydrofuran (2Me-THF); sodium for pentane and toluene; and CaH_2 for dichloromethane (CH_2Cl_2). The NMR experiments were carried out on Bruker DPX-300, DRX-400, DRX-500, and Advance^{III}-400/R spectrometers. The ^1H and ^{13}C spectra were referenced to external $SiMe_4$ using the residual proton peaks of the deuterated solvent as internal standards, while ^{31}P was referenced to external 85% H_3PO_4. NMR signal assignations were made by routine one- and two-dimensional experiments, including ^1H−^1H COSY, ^1H−^1H NOESY, ^1H−^{13}C HSQC, ^1H−^{13}C HMBC, and $^1H\{^{31}P\}$ NMR spectroscopies. All NMR measurements were carried out at 25 °C. Elemental analyses were run by the Analytical Service of the Instituto de Investigaciones Químicas in a Leco TrueSpec CHN elemental analyzer. High resolution mass spectra (HRMS) data were obtained using a Jeol JMS-SX 102A mass spectrometer at the Analytical Services of the Universidad de Sevilla (CITIUS). Infrared spectra were recorded on a Bruker Tensor 27 instrument.

Ir(acac)(COD)[30] and salts **1a**,**b**[14] were synthesized according to reported methods. All other reagents were purchased from commercial suppliers and used as received.

Imidazolium Salt 2a. A solution of **1a** (0.800 g, 2.21 mmol) and ^{t}Bu$_2$PH (1.29 g, 8.80 mmol) in CH_2Cl_2 (20 mL) was heated to 65 °C for 6 days. The solvent was evaporated, and the residue was washed with THF (15 mL), and dried under a vacuum. ScavengePore phenethyl diethylamine (3.500 g; base loading: 0.66 mmol/g) was added to a solution of the solid in CH_2Cl_2 (30 mL), and the mixture was stirred for 1 h and filtered. The solution was brought to dryness, and the residue was washed with Et_2O (15 mL), and dried under a vacuum (0.509 g). The compound was obtained with a purity of 77% as determined by ^1H NMR spectroscopy, and used for the synthesis of the Ir complex **3** without further purification. ^1H NMR (400 MHz, CD_2Cl_2) δ 10.84 (s, 1H, H arom Imid), 8.07 (s, 1H, H arom), 7.65 (m, 2H, 2 H arom), 7.40 (m, 1H, H arom), 7.15 (m, 1H, H arom), 7.04 (m, 2H, 2 H arom Mes), 6.02 (s, 2H, CH_2N), 3.04 (br, 2H, CH_2P), 2.34 (s, 3H, CH_3), 2.07 (s, 6H, 2 CH_3), 1.11 (d, $^3J_{HP}$ = 11.0 Hz, 18H, 2 $C(CH_3)_3$). $^{31}P\{^1H\}$ NMR (162 MHz, CD_2Cl_2) δ 37.1 (br). $^{13}C\{^1H\}$ NMR (101 MHz, CD_2Cl_2) δ 163.2 (C_q arom), 159.2 (C_q arom), 152.5 (C_q arom), 139.4 (CH arom), 138.0 (CH arom),

https://doi.org/10.1021/acs.organomet.1c00109
Organometallics 2021, 40, 1314−1327

134.8 (2 C_q arom), 131.4 (C_q arom), 130.1 (2 CH arom), 124.5 (CH arom), 123.9 (CH arom), 122.7 (CH arom), 121.1 (CH arom), 53.8 (overlapped with the residual solvent signal, CH_2N), 36.5 (d, J_{CP} = 59 Hz, 2 $C(CH_3)_3$), 32.2 (d, J_{CP} = 19 Hz, CH_2P), 29.7 (d, J_{CP} = 12 Hz, 2 $C(CH_3)_3$), 21.2 (CH_3), 17.8 (2 CH_3). HRMS (ESI) m/z 436.2869 $[(M-Cl)^+]$ (exact mass calculated for $C_{27}H_{39}N_3P$: 436.2882).

Imidazolium Salt 2b·HCl. A solution of **1b** (0.700 g, 2.00 mmol) and $^tBu_2PH$ (1.17 g, 8.00 mmol) in CH_2Cl_2 (10 mL) was heated to 65 °C for 6 days. The solvent was evaporated, and the residue was washed with THF (15 mL) and dried under a vacuum giving rise to a light brown solid (0.883 g) that was characterized as the hydrochloride salt of **2b**. The compound was obtained with a purity of 65% as determined by ^1H NMR spectroscopy, and used without further purification for the synthesis of the Ir complex **4**. ^1H NMR (400 MHz, CD_2Cl_2) δ 11.90 (s, 1H, H arom Imid), 8.93 (d, $^1J_{HP}$ = 495 Hz, 1H, PH), 8.89 (s, 1H, H arom Imid), 7.99 (d, $^3J_{HH}$ = 7.6 Hz, 1H, H arom Py), 7.78 (m, 2H, H arom Py + H arom Imid), 7.71 (d, $^3J_{HH}$ = 7.8 Hz, 1H, H arom Py), 7.52 (s, 2H, 2 H arom Xyl), 7.18 (s, 1H, H arom Xyl), 6.06 (s, 2H, CH_2N), 4.01 (d, $^2J_{HP}$ = 12.1 Hz, 2H, CH_2P), 2.44 (s, 6H, 2 CH_3), 1.47 (d, $^3J_{HP}$ = 16.0 Hz, 18H, 2 $C(CH_3)_3$). $^{31}P\{^1H\}$ NMR (162 MHz, CD_2Cl_2) δ 32.5 (br). $^{13}C\{^1H\}$ NMR (101 MHz, CD_2Cl_2) δ 153.0 (C_q arom), 152.5 (d, J_{CP} = 7 Hz, C_q arom), 140.7 (2 C_q arom), 139.3 (CH arom), 137.1 (CH arom), 134.5 (C_q arom), 131.4 (CH arom), 125.0 (CH arom), 124.8 (d, J_{CP} = 6 Hz, CH arom), 123.2 (CH arom), 119.7 (CH arom), 119.0 (2 CH arom), 52.7 (CH_2N), 32.8 (d, J_{CP} = 33 Hz, 2 $C(CH_3)_3$), 27.3 (2 $C(CH_3)_3$), 24.2 (d, J_{CP} = 41 Hz, CH_2P), 21.0 (2 CH_3). HRMS (ESI) m/z 422.2718 $[(M-HCl-Cl)^+]$ (exact mass calculated for $C_{26}H_{37}N_3P$: 422.2725).

Complex 3. A dichloromethane (25 mL) solution of **2a** (0.700 g, 1.38 mmol) and Ir(acac)(COD) (0.495 g, 1.24 mmol) was stirred for 3 days. The formed yellow precipitate was filtered, washed with Et_2O (2 × 10 mL) and pentane (2 × 10 mL), and dried under a vacuum. Light yellow solid (0.431 g, 47%). Crystals of **3** suitable for X-ray diffraction analysis were grown from a saturated solution of the complex in CH_2Cl_2. Anal. Calcd (%) for $C_{27}H_{38}ClIrN_3P$: C 48.89, H 5.78, N 6.34. Found: C 48.99, H 5.94, N 6.06. IR (nujol) 2214 (ν_{IrH}) cm^{-1}. ^1H NMR (500 MHz, CD_2Cl_2) δ 7.64 (s, 1H, H arom NHC), 7.63 (dd, $^3J_{HH}$ = 7.8 Hz, $^3J_{HH}$ = 7.8 Hz, 1H, H arom Py), 7.41 (d, $^3J_{HH}$ = 7.8 Hz, 1H, H arom Py), 7.24 (s, 1H, H arom NHC), 7.20 (d, $^3J_{HH}$ = 7.8 Hz, 1H, H arom Py), 7.07 (d, $^2J_{HH}$ = 14.5 Hz, 1H, C*H*HN), 6.98 (s, 1H, H arom Mes), 6.71 (s, 1H, H arom Mes), 4.90 (d, $^2J_{HH}$ = 14.5 Hz, 1H, C*H*HN), 3.95 (d, $^2J_{HH}$ = 11.3 Hz, 1H, C*H*HIr), 3.58 (dd, $^2J_{HH}$ = 16.5 Hz, $^2J_{HP}$ = 8.7 Hz, 1H, C*H*HP), 2.91 (dd, $^2J_{HH}$ = 11.2 Hz, $^3J_{HP}$ = 9.1 Hz, 1H, CH*H*Ir), 2.70 (dd, $^2J_{HH}$ = 16.5 Hz, $^2J_{HP}$ = 7.2 Hz, 1H, C*H*HP), 2.35 (s, 3H, CH_3 Mes), 2.25 (s, 3H, CH_3 Mes), 1.40 (d, $^3J_{HP}$ = 12.4 Hz, 9H, $C(CH_3)_3$), 1.34 (d, $^3J_{HP}$ = 12.5 Hz, 9H, $C(CH_3)_3$), −24.47 (d, $^2J_{HP}$ = 17.0 Hz, 1H, IrH). $^{31}P\{^1H\}$ NMR (202 MHz, CD_2Cl_2) δ 54.6. $^{13}C\{^1H\}$ NMR (125 MHz, CD_2Cl_2) δ 176.1 (d, J_{CP} = 118 Hz, C-2 NHC), 166.9 (d, J_{CP} = 5 Hz, C_q arom), 156.3 (C_q arom), 151.4 (C_q arom), 136.5 (C_q arom), 135.7 (CH arom), 135.2 (C_q arom), 128.0 (CH arom), 127.7 (C_q arom), 127.2 (CH arom), 122.6 (CH arom), 121.7 (d, J_{CP} = 7 Hz, CH arom), 119.8 (d, J_{CP} = 4 Hz, CH arom), 119.6 (d, J_{CP} = 4 Hz, CH arom), 56.9 (CH_2N), 40.0 (d, J_{CP} = 23 Hz, CH_2P), 38.0 (d, J_{CP} = 9 Hz, $C(CH_3)_3$), 33.2 (d, J_{CP} = 20 Hz, $C(CH_3)_3$), 30.8 (d, J_{CP} = 4 Hz, $C(CH_3)_3$), 29.0 (d, J_{CP} = 5 Hz, $C(CH_3)_3$), 22.2 (CH_3 Mes), 20.9 (CH_3 Mes), −9.6 (br, CH_2Ir).

Complex 4a. In a Fisher−Porter vessel, a suspension of **3** (0.120 g, 0.18 mmol) in CH_2Cl_2 (20 mL) was pressurized with 4 bar of H_2 and heated to 65 °C overnight. The system was depressurized, solvent was evaporated and the residue was washed with pentane (2 × 10 mL). Yellow solid (0.115 g, 96%). Anal. Calcd (%) for $C_{27}H_{40}ClIrN_3P$: C 48.75, H 6.06, N 6.32. Found: C 49.02, H 5.77, N 6.35. IR (nujol) ν = 2235 (ν_{IrH}), 2141 (ν_{IrH}) cm^{-1}. ^1H NMR (400 MHz, CD_2Cl_2) δ 7.69 (dd, $^3J_{HH}$ = 7.8 Hz, $^3J_{HH}$ = 7.8 Hz, 1H, H arom Py), 7.46 (d, $^3J_{HH}$ = 7.8 Hz, 1H, H arom Py), 7.30 (m, 2H, H arom Py + H arom NHC), 7.03 (s, 1H, H arom Mes), 6.95 (d, $^2J_{HH}$ = 14.4 Hz, 1H, C*H*HN), 6.92 (s, 1H, H arom Mes), 6.88 (s, 1H, H arom NHC), 4.92 (d, $^2J_{HH}$ = 14.4 Hz, 1H, C*H*HN), 3.58 (dd, $^2J_{HH}$ = 16.5 Hz, $^2J_{HP}$ = 8.7 Hz, 1H, C*H*HP), 2.78 (dd, $^2J_{HH}$ = 16.5 Hz, $^2J_{HP}$ = 7.6 Hz, 1H, C*H*HP), 2.37 (s, 3H, CH_3), 2.18 (s, 3H, CH_3), 1.92 (s, 3H, CH_3), 1.25 (d, $^3J_{HP}$ = 12.6 Hz, 9H, $C(CH_3)_3$), 1.20 (d, $^3J_{HP}$ = 12.5 Hz, 9H, $C(CH_3)_3$), −20.36 (dd, $^2J_{HP}$ = 14.4 Hz, $^2J_{HH}$ = 6.5 Hz, 1H, IrH *trans* to Py), −24.89 (dd, $^2J_{HP}$ = 17.2 Hz, $^2J_{HH}$ = 6.5 Hz, 1H, IrH *cis* to Py). $^{31}P\{^1H\}$ NMR (122 MHz, CD_2Cl_2) δ 64.8. $^{13}C\{^1H\}$ NMR (101 MHz, CD_2Cl_2) δ 173.2 (d, J_{CP} = 115 Hz, C-2 NHC), 167.0 (d, J_{CP} = 4 Hz, C_q arom), 156.4 (C_q arom), 138.4 (C_q arom), 138.2 (C_q arom), 136.7 (C_q arom), 135.8 (CH arom), 135.4 (C_q arom), 128.9 (CH arom), 128.3 (CH arom), 122.1 (CH arom), 121.5 (d, J_{CP} = 8 Hz, CH arom), 121.0 (d, J_{CP} = 3 Hz, CH arom), 119.8 (d, J_{CP} = 4 Hz, CH arom), 56.5 (CH_2N), 39.4 (d, J_{CP} = 23 Hz, $C(CH_3)$), 38.1 (d, J_{CP} = 10 Hz, CH_2P), 32.4 (d, J_{CP} = 24 Hz, $C(CH_3)$), 30.6 (d, J_{CP} = 3 Hz, 3 $C(CH_3)$), 29.1 (d, J_{CP} = 4 Hz, 3 $C(CH_3)$), 21.3 (CH_3), 18.8 (CH_3), 18.1 (CH_3).

Complexes 4b and 5. Dichloromethane (8 mL) was added to a mixture of **2b·HCl** (0.155 g, 0.31 mmol) and phenethyldiethylamine ScavengePore resin (0.850 g; base loading: 0.66 mmol/g), and the suspension was stirred for 1 h. The mixture was filtered through a short pad of Celite and the solvent was evaporated. A solution of Ir(acac)(COD) (0.125 g, 0.31 mmol) in THF (5 mL) was added to the residue, and the mixture was stirred overnight. The solvent was evaporated, and the resulting solid was washed with pentane (2 × 5 mL). In a Fisher−Porter vessel, a solution of the obtained solid in CH_2Cl_2 (20 mL) was pressurized with 4 bar of H_2, and heated to 65 °C overnight. The system was depressurized, solvent was evaporated, and the residue was washed with pentane (2 × 10 mL). The compounds **4b** and **5**, formed in an approximated ratio of 8:2, were isolated as a yellow solid. Satisfactory elemental analysis for this solid could not be obtained (0.064 g, 32%).

NMR spectroscopy and HRMS data for complex **4b**: ^1H NMR (500 MHz, CD_2Cl_2) δ 7.70 (dd, $^3J_{HH}$ = 7.7 Hz, $^3J_{HH}$ = 7.7 Hz, 1H, H arom Py), 7.47 (d, $^3J_{HH}$ = 7.8 Hz, 1H, H arom Py), 7.28 (m, 3H, 2 H arom Xyl + H arom Py), 7.23 (d, $^3J_{HH}$ = 1.7 Hz, 1H, H arom NHC), 7.17 (d, $^3J_{HH}$ = 1.7 Hz, 1H, H arom NHC), 7.08 (s, 1H, H arom Xyl), 6.94 (d, $^2J_{HH}$ = 14.4 Hz, 1H, C*H*HN), 4.87 (d, $^2J_{HH}$ = 14.4 Hz, 1H, C*H*HN), 3.64 (dd, $^2J_{HH}$ = 16.7 Hz, $^2J_{HP}$ = 8.7 Hz, 1H, C*H*HP), 2.89 (dd, $^2J_{HH}$ = 16.6 Hz, $^2J_{HP}$ = 7.8 Hz, 1H, C*H*HP), 2.39 (s, 6H, 2 CH_3), 1.33 (d, $^3J_{HP}$ = 12.4 Hz, 9H, $C(CH_3)_3$), 1.27 (d, $^3J_{HP}$ = 12.7 Hz, 9H, $C(CH_3)_3$), −20.13 (dd, $^2J_{HP}$ = 14.7 Hz, $^2J_{HH}$ = 6.3 Hz, 1H, IrH *trans* to Py), −24.67 (dd, $^2J_{HP}$ = 17.4 Hz, $^2J_{HH}$ = 6.3 Hz, 1H, IrH *cis* to Py). $^{31}P\{^1H\}$ NMR (162 MHz, THF-d_8) δ 64.6. $^{13}C\{^1H\}$ NMR (101 MHz, THF-d_8) δ 172.2 (d, J_{CP} = 115 Hz, C-2 NHC), 166.7 (C_q arom), 156.9 (C_q arom), 142.7 (C_q arom), 137.6 (2 C_q arom), 136.3 (CH arom), 128.9 (CH arom), 125.8 (2 CH arom), 122.5 (m, 2 CH arom), 121.7 (CH arom), 120.6 (CH arom), 55.8 (CH_2N), 39.3 (d, J_{CP} = 23 Hz, $C(CH_3)_3$), 38.2 (d, J_{CP} = 11 Hz, CH_2P), 33.0 (d, J_{CP} = 24 Hz, $C(CH_3)_3$), 31.0 (3 $C(CH_3)_3$), 29.6 (3 $C(CH_3)_3$), 21.2 (2 Ar−CH_3). HRMS (ESI) m/z 616.2420 $[(M-Cl)^+]$ (exact mass calculated for $C_{26}H_{38}IrN_3P$: 616.2433).

NMR spectroscopy and HRMS data for complex **5**: ^1H NMR (500 MHz, CD_2Cl_2) δ 7.67 (dd, $^3J_{HH}$ = 7.6 Hz, $^3J_{HH}$ = 7.6 Hz, 1H, H arom Py), 7.43 (d, $^3J_{HH}$ = 7.8 Hz, 1H, H arom Py), 7.32 (s, 1H, H arom Xyl), 7.19 (m, 3H, 3 H arom), 6.36 (d, $^2J_{HH}$ = 14.6 Hz, 1H, C*H*HN), 4.30 (m, 1H, C*H*H NHC), 4.17 (d, $^2J_{HH}$ = 14.7 Hz, 1H, C*H*HN), 4.05 (m, 1H, C*H*H NHC), 3.91 (m, 2H, 2 C*H*H NHC), 3.61 (overlapped m, 1H, C*H*HP), 2.88 (overlapped m, 1H, C*H*HP), 2.34 (s, 6H, 2 CH_3), 1.29 (d, $^3J_{HP}$ = 12.0 Hz, 9H, $C(CH_3)_3$), 1.22 (d, $^3J_{HP}$ = 12.8 Hz, 9H, $C(CH_3)_3$), −20.41 (dd, $^2J_{HP}$ = 14.5 Hz, $^2J_{HH}$ = 5.9 Hz, 1H, IrH *trans* to Py), −24.40 (dd, $^2J_{HP}$ = 17.8 Hz, $^2J_{HH}$ = 5.9 Hz, 1H, IrH *cis* to Py). $^{31}P\{^1H\}$ NMR (162 MHz, THF-d_8) δ 64.2. HRMS (ESI) m/z 618.2563 $[(M-Cl)^+]$ (exact mass calculated for $C_{26}H_{40}IrN_3P$: 618.2584).

Complex 6a. Tetrahydrofuran (8 mL) was added to a mixture of complex **4a** (0.095 g, 0.14 mmol) and NaH (0.070 g, 2.9 mmol), and the resulting suspension was heated to 40 °C for 2 days. The solid was filtered off, and the solution was brought to dryness and extracted with Et_2O (2 × 10 mL). The solvent was evaporated, and the residue was extracted with Et_2O (2 × 8 mL) and dried under a vacuum. Yellow solid (0.079 g, 88%). Anal. Calcd (%) for $C_{27}H_{41}IrN_3P$: C

https://doi.org/10.1021/acs.organomet.1c00109
Organometallics 2021, 40, 1314−1327

51.41, H 6.55, N 6.66. Found: C 51.43, H 6.52, N 6.68. IR (nujol) 2101 (ν_{IrH}) cm^{-1}. ^1H NMR (500 MHz, C_6D_6) δ 6.83 (m, 3H, 2 H arom Mes + H arom Py), 6.60 (d, $^3J_{HH}$ = 7.5 Hz, 1H, H arom Py), 6.56 (s, 1H, H arom NHC), 6.40 (d, $^3J_{HH}$ = 7.3 Hz, 1H, H arom Py), 6.34 (s, 1H, H arom NHC), 4.72 (s, 2H, CH_2N), 3.03 (d, $^2J_{HP}$ = 7.9 Hz, 2H, CH_2P), 2.30 (s, 6H, 2 CH_3), 2.11 (s, 3H, CH_3), 1.29 (d, $^3J_{HP}$ = 12.0 Hz, 18H, 2 $C(CH_3)_3$), −10.14 (dd, $^2J_{HP}$ = 15.6 Hz, $^2J_{HH}$ = 5.4 Hz, 2H, 2 IrH *cis* to Py), −20.03 (dt, $^2J_{HP}$ = 13.8 Hz, $^2J_{HH}$ = 5.4 Hz, 1H, IrH *trans* to Py). $^{31}P\{^1H\}$ NMR (202 MHz, C_6D_6) δ 76.3. $^{13}C\{^1H\}$ NMR (126 MHz, C_6D_6) δ 178.8 (d, J_{CP} = 113 Hz, C-2 NHC), 166.8 (d, J_{CP} = 5 Hz, C_q arom), 154.7 (C_q arom), 138.9 (C_q arom), 137.2 (C_q arom), 136.4 (2 C_q arom), 132.1 (CH arom), 128.9 (2 CH arom), 120.0 (CH arom), 119.8 (d, J_{CP} = 8 Hz, CH arom), 119.1 (d, J_{CP} = 4 Hz, CH arom), 118.6 (d, J_{CP} = 3 Hz, CH arom), 59.8 (CH_2N), 41.0 (d, J_{CP} = 19 Hz, CH_2P), 33.2 (d, J_{CP} = 17 Hz, 2 $C(CH_3)$), 29.9 (d, J_{CP} = 5 Hz, 6 $C(CH_3)$), 21.2 (CH_3), 19.6 (2 CH_3).

Complexes 6b and 7. Tetrahydrofuran (8 mL) was added to an 8:2 mixture of complexes **4b** and **5** (0.078 g, 0.12 mmol) and NaH (0.057 g, 2.39 mmol), and the resulting suspension was stirred overnight at room temperature. The solid was filtered through a short pad of Celite, and the solvent was evaporated. The obtained yellow solid was washed with pentane (2 × 8 mL) and dried under a vacuum (0.079 g, 88%). Compounds **6b** and **7** were obtained in an 8:2 ratio. Anal. Calcd (%) for 0.8 $C_{26}H_{39}IrN_3P$ + 0.2 $C_{26}H_{41}IrN_3P$: C 50.60, H 6.43, N 6.81. Found: C 50.23, H 6.78, N 6.46. IR (nujol) 2106 (ν_{IrH}) cm^{-1}.

NMR spectroscopy data for complex **6b**: ^1H NMR (400 MHz, THF-d_8) δ 7.81 (s, 2H, 2 H arom Xyl), 7.56 (dd, $^3J_{HH}$ = 7.6 Hz, $^3J_{HH}$ = 7.6 Hz, 1H, H arom Py), 7.33 (d, $^3J_{HH}$ = 8.1 Hz, 1H, H arom Py), 7.29 (s, 1H, H arom NHC), 7.22 (d, $^3J_{HH}$ = 7.5 Hz, 1H, H arom Py), 7.18 (s, 1H, H arom NHC), 6.88 (s, 1H, H arom Xyl), 5.13 (s, 2H, CH_2N), 3.35 (d, $^2J_{HP}$ = 8.1 Hz, 2H, CH_2P), 2.34 (s, 6H, 2 CH_3), 1.31 (d, $^3J_{HP}$ = 12.0 Hz, 18H, 2 $C(CH_3)_3$), −10.62 (dd, $^2J_{HP}$ = 16.0 Hz, $^2J_{HH}$ = 5.1 Hz, 2H, 2 IrH), −20.37 (dt, $^2J_{HP}$ = 14.6 Hz, $^2J_{HH}$ = 5.0 Hz, 1H, IrH). $^{31}P\{^1H\}$ NMR (162 MHz, THF-d_8) δ 77.3. $^{13}C\{^1H\}$ NMR (101 MHz, THF-d_8) δ 177.8 (d, J_{CP} = 113 Hz, C-2 NHC), 166.3 (d, J_{CP} = 5 Hz, C_q arom), 154.5 (C_q arom), 142.6 (C_q arom), 136.2 (2 C_q arom), 132.7 (CH arom), 127.1 (CH arom), 124.8 (2 CH arom), 119.6 (m, 2 CH arom), 119.2 (d, J_{CP} = 4 Hz, CH arom), 119.1 (CH arom), 59.3 (CH_2N), 40.3 (d, J_{CP} = 20 Hz, CH_2P), 32.6 (d, J_{CP} = 17 Hz, 2 $C(CH_3)$), 29.1 (d, J_{CP} = 5 Hz, 6 $C(CH_3)$), 20.3 (2 CH_3).

NMR spectroscopy data for complex **7**: ^1H NMR (400 MHz, THF-d_8) δ 7.78 (s, 2H, 2 H arom Xyl), 7.53 (dd, $^3J_{HH}$ = 7.5 Hz, $^3J_{HH}$ = 7.5 Hz, 1H, H arom Py), 7.39 (d, $^3J_{HH}$ = 7.4 Hz, 1H, H arom Py), 7.31 (s, 1H, H arom NHC), 7.36 (s, 1H, H arom NHC), 7.12 (d, $^3J_{HH}$ = 7.5 Hz, 1H, H arom Py), 6.68 (s, 1H, H arom Xyl), 4.57 (s, 2H, CH_2N), 3.99 (t, $^3J_{HH}$ = 8.5 Hz, 2H, CH_2CH_2), 3.76 (t, $^3J_{HH}$ = 8.7 Hz, 2H, CH_2CH_2), 3.35 (d, $^2J_{HP}$ = 8.1 Hz, 2H, CH_2P), 2.28 (s, 6H, 2 CH_3), 1.23 (d, $^3J_{HP}$ = 12.9 Hz, 18H, 2 $C(CH_3)_3$), −10.56 (dd, $^2J_{HP}$ = 17.6 Hz, $^2J_{HH}$ = 5.0 Hz, 2H, 2 IrH), −20.65 (dt, $^2J_{HP}$ = 14.2 Hz, $^2J_{HH}$ = 5.0 Hz, 1H, IrH). $^{31}P\{^1H\}$ NMR (162 MHz, THF-d_8) δ 76.5.

Complexes $8a^M$/$8a^m$. In a J. Young valved NMR tube, a solution of **4a** (0.020 g, 0.030 mmol) in THF-d_8 (0.5 mL) was treated with KHMDS (0.008 g, 0.039 mmol) and benzaldehyde (6.0 μL, 0.060 mmol). The resulting solution was analyzed by NMR spectroscopy.

NMR spectroscopy data for complex $\mathbf{8a^M}$: ^1H NMR (500 MHz, THF-d_8) δ 7.74 (t, $^3J_{HH}$ = 7.6 Hz, 1H, H arom), 7.62 (t, $^3J_{HH}$ = 7.4 Hz, 1H, H arom), 7.53 (m, H arom), 7.43 (m, 2 H arom), 7.04 (m, 2H, 2 H arom), 6.91 (m, 2H, 2 H arom), 6.80 (s, 1H, H arom), 6.75 (s, 1H, H arom), 6.59 (s, 1H, H arom), 5.64 (s, 1H, CHN), 4.90 (s, 1H, CHOIr), 3.61 (d, $^2J_{HH}$ = 15.5 Hz, $^2J_{HP}$ = 8.9 Hz, 1H, C*H*HP), 2.95 (dd, $^2J_{HH}$ = 15.5 Hz, $^2J_{HP}$ = 6.7 Hz, 1H, C*H*HP), 2.28 (s, 3H, CH_3), 2.21 (s, 3H, CH_3), 1.74 (s, 3H, CH_3), 1.23 (d, $^3J_{HP}$ = 12.1 Hz, 9H, $C(CH_3)_3$), 1.05 (d, $^3J_{HP}$ = 12.1 Hz, 9H, $C(CH_3)_3$), −19.39 (dd, $^2J_{HP}$ = 14.2 Hz, $^2J_{HH}$ = 7.8 Hz, 1H, IrH *trans* to Py), −24.33 (dd, $^2J_{HP}$ = 18.2 Hz, $^2J_{HH}$ = 7.8 Hz, 1H, IrH *cis* to Py). $^{31}P\{^1H\}$ NMR (162 MHz, THF-d_8) δ 75.5. $^{13}C\{^1H\}$ NMR (101 MHz, THF-d_8) δ 176.7 (d, J_{CP} = 119 Hz, C-2 NHC), 166.6 (d, J_{CP} = 5 Hz, C_q arom), 158.9 (C_q arom), 150.4 (C_q arom), 138.5 (C_q arom), 137.8 (C_q arom), 136.7 (C_q arom), 136.2 (C_q arom), 135.9 (CH arom), 129.2 (CH arom), 128.4 (CH arom), 127.8 (2 CH arom), 127.2 (2 CH arom), 125.6 (CH arom), 120.9 (d, J_{CP} = 2 Hz, CH arom), 120.7 (d, J_{CP} = 7 Hz, CH arom), 120.0 (CH arom), 119.4 (d, J_{CP} = 3 Hz, CH arom), 76.8 (CHN), 75.4 (CHOIr), 39.6 (d, J_{CP} = 21 Hz, $C(CH_3)$), 36.8 (d, J_{CP} = 7 Hz, CH_2P), 31.9 (d, J_{CP} = 23 Hz, $C(CH_3)$), 30.6 (d, J_{CP} = 3 Hz, 3 $C(CH_3)$), 29.5 (d, J_{CP} = 5 Hz, 3 $C(CH_3)$), 21.0 (CH_3), 19.1 (CH_3), 18.2 (CH_3).

Diagnostic NMR spectroscopy data for complex $\mathbf{8a^m}$: ^1H NMR (500 MHz, THF-d_8) δ −20.06 (dd, $^2J_{HP}$ = 13.7 Hz, $^2J_{HH}$ = 7.4 Hz, 1H, IrH *trans* to Py), −24.11 (dd, $^2J_{HP}$ = 18.5 Hz, $^2J_{HH}$ = 7.4 Hz, 1H, IrH *cis* to Py). $^{31}P\{^1H\}$ NMR (162 MHz, THF-d_8) δ 76.1.

Complexes $8b^M$/$8b^m$. In a J. Young valved NMR tube, a solution of **4a** (0.010 g, 0.015 mmol) in THF-d_8 (0.5 mL) was treated with KHMDS (0.004 g, 0.020 mmol) and *p*-bromobenzaldehyde (0.004 g, 0.022 mmol). The resulting solution was analyzed by NMR spectroscopy.

NMR spectroscopy data for complex $\mathbf{8b^M}$: ^1H NMR (500 MHz, THF-d_8) δ 7.78 (dd, $^3J_{HH}$ = 8.0 Hz, $^3J_{HH}$ = 8.0 Hz, 1H, H arom Py), 7.54 (d, $^3J_{HH}$ = 8.0 Hz, H arom Py), 7.44 (d, $^3J_{HH}$ = 8.1 Hz, H arom Py), 7.36 (d, $^3J_{HH}$ = 8.1 Hz, 2H, 2 H arom *p*-BrPh), 7.19 (d, $^3J_{HH}$ = 8.1 Hz, 2H, 2 H arom *p*-BrPh), 6.95 (s, 1H, H arom), 6.81 (s, 2H, 2 H arom), 6.66 (s, 1H, H arom), 5.62 (s, 1H, CHN), 4.87 (s, 1H, CHOIr), 3.61 (d, $^2J_{HH}$ = 15.6 Hz, $^2J_{HP}$ = 8.8 Hz, 1H, C*H*HP), 2.95 (dd, $^2J_{HH}$ = 15.6 Hz, $^2J_{HP}$ = 6.7 Hz, 1H, C*H*HP), 2.28 (s, 3H, CH_3), 2.18 (s, 3H, CH_3), 1.74 (s, 3H, CH_3), 1.22 (d, $^3J_{HP}$ = 12.1 Hz, 9H, $C(CH_3)_3$), 1.03 (d, $^3J_{HP}$ = 12.3 Hz, 9H, $C(CH_3)_3$), −19.39 (dd, $^2J_{HP}$ = 14.2 Hz, $^2J_{HH}$ = 7.8 Hz, 1H, IrH *trans* to Py), −24.48 (dd, $^2J_{HP}$ = 18.4 Hz, $^2J_{HH}$ = 7.8 Hz, 1H, IrH *cis* to Py). $^{31}P\{^1H\}$ NMR (202 MHz, THF-d_8) δ 75.6. $^{13}C\{^1H\}$ NMR (101 MHz, THF-d_8) δ 166.9 (d, J_{CP} = 4 Hz, C_q arom), 158.7 (C_q arom), 149.8 (C_q arom), 138.6 (C_q arom), 138.0 (C_q arom), 136.7 (C_q arom), 136.3 (C_q arom), 136.2 (CH arom), 130.4 (2 CH arom), 130.0 (2 CH arom), 129.2 (CH arom), 128.6 (CH arom), 121.1 (m, 2 CH arom), 120.3 (CH arom), 120.0 (CH arom), 119.4 (C_q arom), 76.5 (CHN), 75.0 (CHOIr), 39.8 (d, J_{CP} = 21 Hz, $C(CH_3)$), 36.9 (d, J_{CP} = 7 Hz, CH_2P), 32.1 (d, J_{CP} = 23 Hz, $C(CH_3)$), 30.8 (d, J_{CP} = 3 Hz, 3 $C(CH_3)$), 29.6 (d, J_{CP} = 4 Hz, 3 $C(CH_3)$), 21.2 (CH_3), 19.2 (CH_3), 18.3 (CH_3) ppm; signal of the C2-NHC carbon could not be detected due to the low solubility of complex $\mathbf{8b^M}$. This signal was determined to appear at 176.0 ppm from the $^1H-^{13}C$ HBQC experiment.

Diagnostic NMR spectroscopy data for complex $\mathbf{8b^m}$: ^1H NMR (500 MHz, THF-d_8) δ −20.01 (dd, $^2J_{HP}$ = 14.0 Hz, $^2J_{HH}$ = 7.7 Hz, 1H, IrH *trans* to Py), −24.34 (dd, $^2J_{HP}$ = 19.5 Hz, $^2J_{HH}$ = 7.7 Hz, 1H, IrH *cis* to Py). $^{31}P\{^1H\}$ NMR (162 MHz, THF-d_8) δ 76.1.

Complex 9. A solution of **4a** (0.070 g, 0.105 mmol) in THF (5 mL) was treated with KHMDS (0.022 g, 0.110 mmol) and benzaldehyde (32 μL, 0.315 mmol). The suspension was filtered through a short pad of Celite. Water (50 μL) was added, and the resulting solution was heated to 60 °C for 6 h. The reaction mixture was brought to dryness, and the residue was washed with Et_2O (3 × 5 mL) and cold THF (3 mL). Yellow solid (0.047 g, 60%). Anal. Calcd (%) for $C_{34}H_{45}IrN_3O_2P$: C 54.38, H 6.04, N 5.60. Found: C 54.42, H 5.96, N 5.36. IR (nujol) 1601 ($\nu_{as,\ COO}$) cm^{-1}. ^1H NMR (400 MHz, CD_2Cl_2) δ 7.81 (d, $^3J_{HH}$ = 7.0 Hz, 2H, 2 H arom), 7.69 (t, $^3J_{HH}$ = 7.7 Hz, 1H, H arom), 7.45 (d, $^3J_{HH}$ = 7.6 Hz, 1H, H arom), 7.22 (m, 5H, 5 H arom), 7.01 (s, 1H, H arom), 6.85 (s, 2H, 2 H arom), 6.13 (d, $^2J_{HH}$ = 14.6 Hz, 1H, C*H*HN), 4.85 (d, $^2J_{HH}$ = 14.6 Hz, 1H, C*H*HN), 3.56 (dd, $^2J_{HH}$ = 16.7 Hz, $^2J_{HP}$ = 8.8 Hz, 1H, C*H*HP), 2.81 (dd, $^2J_{HH}$ = 16.7 Hz, $^2J_{HP}$ = 7.5 Hz, 1H, C*H*HP), 2.33 (s, 3H, CH_3), 2.31 (s, 3H, CH_3), 1.82 (s, 3H, CH_3), 1.18 (d, $^3J_{HP}$ = 12.5 Hz, 18H, 2 $C(CH_3)_3$), −19.91 (dd, $^2J_{HP}$ = 14.4 Hz, $^2J_{HH}$ = 6.7 Hz, 1H, IrH *trans* to Py), −26.85 (dd, $^2J_{HP}$ = 17.1 Hz, $^2J_{HH}$ = 6.7 Hz, 1H, IrH *cis* to Py). $^{31}P\{^1H\}$ NMR (122 MHz, CD_2Cl_2) δ 63.0. $^{13}C\{^1H\}$ NMR (101 MHz, CD_2Cl_2) δ 174.7 (d, J_{CP} = 116 Hz, C-2 NHC), 171.0 (Ir-CO_2Ph), 167.3 (C_q arom), 156.5 (C_q arom), 138.9 (C_q arom), 138.4 (C_q arom), 138.0 (C_q arom), 137.2 (C_q arom), 135.7 (CH arom + C_q arom), 129.7 (2 CH arom), 129.0 (CH arom), 128.9 (CH arom), 128.1 (CH arom), 127.4 (2 CH arom), 121.9 (CH arom), 121.6 (d, J_{CP} = 8 Hz, CH arom), 120.4 (CH arom), 119.9 (CH arom), 56.8 (CH_2N), 39.1 (d, J_{CP} = 22 Hz, $C(CH_3)$), 36.8 (d, J_{CP} = 9 Hz, CH_2P),

https://doi.org/10.1021/acs.organomet.1c00109
Organometallics 2021, 40, 1314−1327

32.3 (d, J_{CP} = 25 Hz, $C(CH_3)$), 30.4 (3 $C(CH_3)$), 29.1 (3 $C(CH_3)$), 21.2 (CH_3), 18.7 (CH_3), 18.1 (CH_3).

Representative Procedure for Aldehyde Hydrogenation. In a glovebox, a Fisher−Porter vessel was charged with a solution of complex **6a** (1.0 mg, 1.6 μmol) and benzaldehyde (162 μL, 1.6 mmol) in 2-methyltetrahydrofuran (0.8 mL). The reactor was purged three times with H_2, and finally pressurized with 4 bar of H_2. After 24 h, the reactor was depressurized, the reaction solution was evaporated, and conversion and selectivity were determined by ^{1}H NMR spectroscopy using mesitylene as internal standard.

DFT Calculations. Calculations were carried out at the DFT level using the Gaussian 09 program[31] with the B3LYP hybrid functional,[32] with dispersion effects taken into account by adding the D3 version of Grimmés empirical dispersion.[33] All atoms were represented with the 6-31g(d,p) basis set,[34] except Ir, for which the Stuttgart/Dresden Effective Core Potential and its associated basis set SDD[35] was used. All geometry optimizations were performed in bulk solvent (THF) without restrictions. Vibrational analysis was used to characterize the stationary points in the potential energy surface, as well as for calculating the zero-point, enthalpy, and Gibbs energy corrections at 295 K and 1 atm. The nature of the intermediates connected by a given transition state along a reaction path was proven by intrinsic reaction coordinate (IRC) calculations or by perturbing the geometry of the TS along the reaction path eigenvector. Bulk solvent effects were modeled with the SMD continuum model.[36]

X-ray Structure Analysis of Complexes 3, 8b^M, and 9. Crystals suitable for X-ray diffraction analysis were coated with dry perfluoropolyether, mounted on glass fibers, and fixed in a cold nitrogen stream to the goniometer head. Data collections were performed on a Bruker-Nonius X8 Apex-II CCD (**3**) and on a Bruker-AXS, D8 QUEST ECO, PHOTON II area detector (**8b^M** and **9**) diffractometers, using graphite monochromatized Mo radiation (λ(Mo Kα) = 0.71073 Å) and fine-sliced ω and φ scans (scan widths 0.30° to 0.50°).[37] The data were reduced (*SAINT*) and corrected for absorption effects by the multiscan method (*SADABS*).[38] The structures were solved by direct methods (*SIR2002*, *SHELXS*) and refined against all F^2 data by full-matrix least-squares techniques [*SHELXL*-2016/6 (**3**) and *SHELXL*-2018/3 (**8b^M** and **9**)] minimizing $w[F_0^2 - F_c^2]^2$.[39] All non-hydrogen atoms were refined with anisotropic displacement parameters. Hydrogen atoms were included in calculated positions and allowed to ride on their carrier atoms with the isotropic temperature factors U_{iso} fixed at 1.2 times (1.5 times for methyl groups) of the U_{eq} values of the respective carrier atoms. The asymmetric unit of **3** presents one iridium complex and two dichloromethane molecules of crystallization. The asymmetric unit of **8b^M** presents two symmetrically independent enantiomers (*R*,*R*) and (*S*,*S*) (a racemate) of the complex of Ir (III) with the anionic tetrahapto pincer ligand coordinated to the iridium atom together with two hydrides in cis. A search for solvent accessible voids for the crystal structure of **8b^M** using *PLATON*,[40] showed two small volumes of potential solvents of 1111 Å^3 for each (305 electron count for each), whose solvent content could not be identified or refined with the most severe restraints. The corresponding CIF data represent *SQUEEZE*[41] treated structures with the solvent molecules handling as a diffuse contribution to the overall scattering, without specific atom position and excluded from the structural model. The *SQUEEZE* results were appended to the CIF. The asymmetric unit of **9** presents one iridium complex and two toluene molecules of crystallization without showing disorder. A summary of cell parameters, data collection, structures solution, and the refinement of crystal structures are provided in the Supporting Information. The corresponding crystallographic data were deposited with the Cambridge Crystallographic Data Centre as supplementary publications. CCDC 2064071 (**3**), 2064072 (**8b^M**), and 2064073 (**9**). The data can be obtained free of charge via https://www.ccdc.cam.ac.uk/structures/.

■ ASSOCIATED CONTENT

Supporting Information

The Supporting Information is available free of charge at https://pubs.acs.org/doi/10.1021/acs.organomet.1c00109.

Experimental details, selected NMR spectra, X-ray diffraction data, and DFT calculations (PDF)
DFT calculations coordinates (XYZ)

Accession Codes

CCDC 2064071−2064073 contain the supplementary crystallographic data for this paper. These data can be obtained free of charge via www.ccdc.cam.ac.uk/data_request/cif, or by emailing data_request@ccdc.cam.ac.uk, or by contacting The Cambridge Crystallographic Data Centre, 12 Union Road, Cambridge CB2 1EZ, UK; fax: +44 1223 336033.

■ AUTHOR INFORMATION

Corresponding Authors

Nuria Rendón − *Instituto de Investigaciones Químicas (IIQ), Departamento de Química Inorgánica and Centro de Innovación en Química Avanzada (ORFEO−CINQA), CSIC and Universidad de Sevilla, 41092 Sevilla, Spain*; Email: nuria@iiq.csic.es

Andrés Suárez − *Instituto de Investigaciones Químicas (IIQ), Departamento de Química Inorgánica and Centro de Innovación en Química Avanzada (ORFEO−CINQA), CSIC and Universidad de Sevilla, 41092 Sevilla, Spain*; Email: andres.suarez@iiq.csic.es

Authors

Práxedes Sánchez − *Instituto de Investigaciones Químicas (IIQ), Departamento de Química Inorgánica and Centro de Innovación en Química Avanzada (ORFEO−CINQA), CSIC and Universidad de Sevilla, 41092 Sevilla, Spain*

Martín Hernández-Juárez − *Centro de Investigaciones Químicas, Universidad Autónoma del Estado de Hidalgo (UAEH), C.P. 42184 Mineral de la Reforma, Hidalgo, Mexico*

Joaquín López-Serrano − *Instituto de Investigaciones Químicas (IIQ), Departamento de Química Inorgánica and Centro de Innovación en Química Avanzada (ORFEO−CINQA), CSIC and Universidad de Sevilla, 41092 Sevilla, Spain*

Eleuterio Álvarez − *Instituto de Investigaciones Químicas (IIQ), Departamento de Química Inorgánica and Centro de Innovación en Química Avanzada (ORFEO−CINQA), CSIC and Universidad de Sevilla, 41092 Sevilla, Spain*

Margarita Paneque − *Instituto de Investigaciones Químicas (IIQ), Departamento de Química Inorgánica and Centro de Innovación en Química Avanzada (ORFEO−CINQA), CSIC and Universidad de Sevilla, 41092 Sevilla, Spain*; orcid.org/0000-0002-8055-2491

Complete contact information is available at: https://pubs.acs.org/10.1021/acs.organomet.1c00109

Notes

The authors declare no competing financial interest.

■ ACKNOWLEDGMENTS

Dedicated to Prof. Maurizio Peruzzini on the occasion of his 65th anniversary. Financial support (FEDER contribution) from the Spanish MINECO and AEI (CTQ2016-80814-R and PID2019-104159GB-I00/AEI/10.13039/501100011033) and

Junta de Andalucía (P18-FR-3208) is gratefully acknowledged. We are thankful for the use of computational facilities of the Supercomputing Center of Galicia (CESGA).

REFERENCES

(1) Khusnutdinova, J. R.; Milstein, D. Metal-Ligand Cooperation. *Angew. Chem., Int. Ed.* **2015**, *54*, 12236−12273.

(2) (a) Milstein, D. Metal-Ligand Cooperation by Aromatization-Dearomatization as a Tool in Single Bond Activation. *Philos. Trans. R. Soc., A* **2015**, *373*, 20140189. (b) Shimbayashi, T.; Fujita, K. Recent Advances in Homogeneous Catalysis via Metal-Ligand Cooperation Involving Aromatization and Dearomatization. *Catalysts* **2020**, *10*, 635.

(3) (a) Filonenko, G. A.; Cosimi, E.; Lefort, L.; Conley, M. P.; Copéret, C.; Lutz, M.; Hensen, E. J. M.; Pidko, E. A. Lutidine-Derived Ru-CNC Hydrogenation Pincer Catalysts with Versatile Coordination Properties. *ACS Catal.* **2014**, *4*, 2667−2671. (b) Filonenko, G. A.; Smykowski, D.; Szyja, B. M.; Li, G.; Szczygiel, J.; Hensen, E. J. M.; Pidko, E. A. Catalytic Hydrogenation of CO_2 to Formates by a Lutidine-Derived Ru-CNC Pincer Complex: Theoretical Insight into the Unrealized Potential. *ACS Catal.* **2015**, *5*, 1145−1154.

(4) (a) Sun, Y.; Koehler, C.; Tan, R.; Annibale, V. T.; Song, D. Ester Hydrogenation Catalyzed by Ru-CNN Pincer Complexes. *Chem. Commun.* **2011**, *47*, 8349−8351. (b) Del Pozo, C.; Iglesias, M.; Sánchez, F. Pincer-Type Pyridine-Based N-Heterocyclic Carbene Amine Ru(II) Complexes as Efficient Catalysts for Hydrogen Transfer Reactions. *Organometallics* **2011**, *30*, 2180−2188. (c) Fogler, E.; Balaraman, E.; Ben-David, Y.; Leitus, G.; Shimon, L. J. W.; Milstein, D. New CNN-Type Ruthenium Pincer NHC Complexes. Mild, Efficient Catalytic Hydrogenation of Esters. *Organometallics* **2011**, *30*, 3826−3833.

(5) (a) Hernández-Juárez, M.; Vaquero, M.; Álvarez, E.; Salazar, V.; Suárez, A. Hydrogenation of Imines Catalysed by Ruthenium(II) Complexes Based on Lutidine-Derived CNC Pincer Ligands. *Dalton Trans.* **2013**, *42*, 351−354. (b) Hernández-Juárez, M.; López-Serrano, J.; Lara, P.; Morales-Cerón, J. P.; Vaquero, M.; Álvarez, E.; Salazar, V.; Suárez, A. Ruthenium(II) Complexes Containing Lutidine-Derived Pincer CNC Ligands: Synthesis, Structure, and Catalytic Hydrogenation of C-N Bonds. *Chem. - Eur. J.* **2015**, *21*, 7540−7555.

(6) (a) Toda, T.; Kuwata, S.; Ikariya, T. Unsymmetrical Pincer-Type Ruthenium Complex Containing β-Protic Pyrazole and N-Heterocyclic Carbene Arms: Comparison of Brønsted Acidity of NH Groups in Second Coordination Sphere. *Chem. - Eur. J.* **2014**, *20*, 9539−9542. (b) Toda, T.; Yoshinari, A.; Ikariya, T.; Kuwata, S. Protic N-Heterocyclic Carbene Versus Pyrazole: Rigorous Comparison of Proton- and Electron-Donating Abilities in a Pincer-Type Framework. *Chem. - Eur. J.* **2016**, *22*, 16675−16683. (c) Tang, Z.; Otten, E.; Reek, J. N. H.; van der Vlugt, J. I.; de Bruin, B. Dynamic Ligand Reactivity in a Rhodium Pincer Complex. *Chem. - Eur. J.* **2015**, *21*, 12683−12693. (d) Polezhaev, A. V.; Chen, C.-H.; Losovyj, Y.; Caulton, K. G. A Multifunctional Pincer Ligand Supports Unsaturated Cobalt: Five Functionalities in One Pincer. *Chem. - Eur. J.* **2017**, *23*, 8039−8050. (e) Polezhaev, A. V.; Liss, C. J.; Telser, J.; Chen, C.-H.; Caulton, K. G. A PNNH Pincer Ligand Allows Access to Monovalent Iron. *Chem. - Eur. J.* **2018**, *24*, 1330−1341.

(7) (a) Fogler, E.; Garg, J. A.; Hu, P.; Leitus, G.; Shimon, L. J. W.; Milstein, D. System with Potential Dual Modes of Metal-Ligand Cooperation: Highly Catalytically Active Pyridine-Based PNNH-Ru Pincer Complexes. *Chem. - Eur. J.* **2014**, *20*, 15727−15731. (b) Kar, S.; Rauch, M.; Kumar, A.; Leitus, G.; Ben-David, Y.; Milstein, D. Selective Room-Temperature Hydrogenation of Amides to Amines and Alcohols Catalyzed by a Ruthenium Pincer Complex and Mechanistic Insight. *ACS Catal.* **2020**, *10*, 5511−5515. (c) Hu, P.; Fogler, E.; Diskin-Posner, Y.; Iron, M. A.; Milstein, D. A Novel Liquid Organic Hydrogen Carrier System Based on Catalytic Peptide Formation and Hydrogenation. *Nat. Commun.* **2015**, *6*, 6859. (d) Kumar, A.; Janes, T.; Espinosa-Jalapa, N. A.; Milstein, D. Selective Hydrogenation of Cyclic Imides to Diols and Amines and Its Application in the Development of a Liquid Organic Hydrogen Carrier. *J. Am. Chem. Soc.* **2018**, *140*, 7453−7457. (e) Srimani, D.; Mukherjee, A.; Goldberg, A. F. G.; Leitus, G.; Diskin-Posner, Y.; Shimon, L. J. W.; Ben-David, Y.; Milstein, D. Cobalt-Catalyzed Hydrogenation of Esters to Alcohols: Unexpected Reactivity Trend Indicates Ester Enolate Intermediacy. *Angew. Chem., Int. Ed.* **2015**, *54*, 12357−12360. (f) Mukherjee, A.; Srimani, D.; Chakraborty, S.; Ben-David, Y.; Milstein, D. Selective Hydrogenation of Nitriles to Primary Amines Catalyzed by a Cobalt Pincer Complex. *J. Am. Chem. Soc.* **2015**, *137*, 8888−8891. (g) Daw, P.; Chakraborty, S.; Garg, J. A.; Ben-David, Y.; Milstein, D. Direct Synthesis of Pyrroles by Dehydrogenative Coupling of Diols and Amines Catalyzed by Cobalt Pincer Complexes. *Angew. Chem., Int. Ed.* **2016**, *55*, 14373−14377. (h) Daw, P.; Ben-David, Y.; Milstein, D. Direct Synthesis of Benzimidazoles by Dehydrogenative Coupling of Aromatic Diamines and Alcohols Catalyzed by Cobalt. *ACS Catal.* **2017**, *7*, 7456−7460. (i) Espinosa-Jalapa, N. A.; Nerush, A.; Shimon, L. J. W.; Leitus, G.; Avram, L.; Ben-David, Y.; Milstein, D. Manganese-Catalyzed Hydrogenation of Esters to Alcohols. *Chem. - Eur. J.* **2017**, *23*, 5934−5938. (j) Kumar, A.; Janes, T.; Espinosa-Jalapa, N. A.; Milstein, D. Manganese Catalyzed Hydrogenation of Organic Carbonates to Methanol and Alcohols. *Angew. Chem., Int. Ed.* **2018**, *57*, 12076−12080. (k) Kumar, A.; Espinosa-Jalapa, N. A.; Leitus, G.; Diskin-Posner, Y.; Avram, L.; Milstein, D. Direct Synthesis of Amides by Dehydrogenative Coupling of Amines with either Alcohols or Esters: Manganese Pincer Complex as Catalyst. *Angew. Chem., Int. Ed.* **2017**, *56*, 14992−14996. (l) Espinosa-Jalapa, N. A.; Kumar, A.; Leitus, G.; Diskin-Posner, Y.; Milstein, D. Synthesis of Cyclic Imides by Acceptorless Dehydrogenative Coupling of Diols and Amines Catalyzed by a Manganese Pincer Complex. *J. Am. Chem. Soc.* **2017**, *139*, 11722−11725. (m) Zou, Y.-Q.; Zhou, Q.-Q.; Diskin-Posner, Y.; Ben-David, Y.; Milstein, D. Synthesis of Oxalamides by Acceptorless Dehydrogenative Coupling of Ethylene Glycol and Amines and the Reverse Hydrogenation Catalyzed by Ruthenium. *Chem. Sci.* **2020**, *11*, 7188−7193. (n) Xie, Y.; Hu, P.; Ben-David, Y.; Milstein, D. A Reversible Liquid Organic Hydrogen Carrier System Based on Methanol-Ethylenediamine and Ethylene Urea. *Angew. Chem., Int. Ed.* **2019**, *58*, 5105−5109. (o) Zou, Y.-Q.; von Wolff, N.; Anaby, A.; Xie, Y.; Milstein, D. Ethylene Glycol as an Efficient and Reversible Liquid Organic Hydrogen Carrier. *Nat. Catal.* **2019**, *2*, 415−422.

(8) (a) Tan, X.; Wang, Y.; Liu, Y.; Wang, F.; Shi, L.; Lee, K.-H.; Lin, Z.; Lv, H.; Zhang, X. Highly Efficient Tetradentate Ruthenium Catalyst for Ester Reduction: Especially for Hydrogenation of Fatty Acid Esters. *Org. Lett.* **2015**, *17*, 454−457. (b) Shi, L.; Tan, X.; Long, J.; Xiong, X.; Yang, S.; Xue, P.; Lv, H.; Zhang, X. Direct Catalytic Hydrogenation of Simple Amides: A Highly Efficient Approach from Amides to Amines and Alcohols. *Chem. - Eur. J.* **2017**, *23*, 546−548.

(9) (a) Sánchez, P.; Hernández-Juárez, M.; Rendón, N.; López-Serrano, J.; Santos, L. L.; Álvarez, E.; Paneque, M.; Suárez, A. Hydrogenation/Dehydrogenation of N-Heterocycles Catalyzed by Ruthenium Complexes Based on Multimodal Proton-Responsive CNN(H) Pincer Ligands. *Dalton Trans.* **2020**, *49*, 9583−9587. (b) Wu, X.; Ji, L.; Ji, Y.; Elageed, E. H. M.; Gao, G. Hydrogenation of Ethylene Carbonate Catalyzed by Lutidine-Bridged N-Heterocyclic Carbene Ligands and Ruthenium Precursors. *Catal. Commun.* **2016**, *85*, 57−60.

(10) Zhao, B.; Han, Z.; Ding, K. The N-H Functional Group in Organometallic Catalysis. *Angew. Chem., Int. Ed.* **2013**, *52*, 4744−4788.

(11) (a) De Boer, S. Y.; Korstanje, T. J.; La Rooij, S. R.; Kox, R.; Reek, J. N. H.; van der Vlugt, J. I. Ruthenium PNN(O) Complexes: Cooperative Reactivity and Application as Catalysts for Acceptorless Dehydrogenative Coupling Reactions. *Organometallics* **2017**, *36*, 1541−1549. (b) Huang, M.; Li, Y.; Liu, J.; Lan, X.-B.; Liu, Y.; Zhao, C.; Ke, Z. A Bifunctional Strategy for N-Heterocyclic Carbene-Stabilized Iridium Complex-Catalyzed N-Alkylation of Amines with Alcohols in Aqueous Media. *Green Chem.* **2019**, *21*, 219−224.

https://doi.org/10.1021/acs.organomet.1c00109
Organometallics 2021, 40, 1314−1327

(12) Hou, C.; Jiang, J.; Li, Y.; Zhao, C.; Ke, Z. When Bifunctional Catalyst Encounters Dual MLC Modes: DFT Study on the Mechanistic Preference in Ru-PNNH Pincer Complex Catalyzed Dehydrogenative Coupling Reaction. *ACS Catal.* **2017**, *7*, 786−795.
(13) Asay, M.; Morales-Morales, D. Non-Symmetric Pincer Ligands: Complexes and Applications in Catalysis. *Dalton Trans.* **2015**, *44*, 17432−17447.
(14) Sánchez, P.; Hernández-Juárez, M.; Álvarez, E.; Paneque, M.; Rendón, N.; Suárez, A. Synthesis, Structure and Reactivity of Pd and Ir Complexes Based on New Lutidine-Derived NHC/Phosphine Mixed Pincer Ligands. *Dalton Trans.* **2016**, *45*, 16997−17009.
(15) (a) Hernández-Juárez, M.; López-Serrano, J.; González-Herrero, P.; Rendón, N.; Álvarez, E.; Paneque, M.; Suárez, A. Hydrogenation of an Iridium-Coordinated Imidazol-2-ylidene Ligand Fragment. *Chem. Commun.* **2018**, *54*, 3843−3846. (b) Hernández-Juárez, M.; Sánchez, P.; López-Serrano, J.; Lara, P.; González-Herrero, P.; Rendón, N.; Álvarez, E.; Paneque, M.; Suárez, A. Metalated Ir-CNP Complexes Containing Imidazolin-2-ylidene and Imidazolidin-2-ylidene Donors - Synthesis, Structure, Luminescence, and Metal-Ligand Cooperative Reactivity. *Eur. J. Inorg. Chem.* **2020**, *2020*, 3944−3953.
(16) Sánchez, P.; Hernández-Juárez, M.; Rendón, N.; López-Serrano, J.; Álvarez, E.; Paneque, M.; Suárez, A. Hydroboration of Carbon Dioxide with Catechol and Pinacol Borane Using an Ir-CNP* Pincer Complex. Water Influence on the Catalytic Activity. *Dalton Trans.* **2018**, *47*, 16766−16776.
(17) (a) Clarke, M. L.; Roff, G. J. Homogeneous Hydrogenation of Aldehydes, Ketones, Imines and Carboxylic Acid Derivatives: Chemoselectivity and Catalytic Activity. In *The Handbook of Homogeneous Hydrogenation*; de Vries, J. G., Elsevier, C. J., Eds.; Wiley-VCH, 2007; Chapter 15, Vol. *1*. (b) Magano, J.; Dunetz, J. R. Large-Scale Carbonyl Reductions in the Pharmaceutical Industry. *Org. Process Res. Dev.* **2012**, *16*, 1156−1184.
(18) (a) Garhwal, S.; Maji, B.; Semwal, S.; Choudhury, J. Ambient-Pressure and Base-Free Aldehyde Hydrogenation Catalyst Supported by a Bifunctional Abnormal NHC Ligand. *Organometallics* **2018**, *37*, 4720−4725. (b) Wang, R.; Qi, J.; Yue, Y.; Lian, Z.; Xiao, H.; Zhuo, S.; Xing, L. Ambient-Pressure Hydrogenation of Ketones and Aldehydes by a Metal-Ligand Bifunctional Catalyst [Cp*Ir(2,2′-bpyO)(H_2O)] without Using Base. *Tetrahedron* **2019**, *75*, 130463. (c) Chen, X.; Jia, W.; Guo, R.; Graham, T. W.; Gullons, M. A.; Abdur-Rashid, K. Highly Active Iridium Catalysts for the Hydrogenation of Ketones and Aldehydes. *Dalton Trans.* **2009**, 1407−1410. (d) Chaplin, A. B.; Dyson, P. J. Catalytic Activity of Bis-phosphine Ruthenium(II)-Arene Compounds: Chemoselective Hydrogenation and Mechanistic Insights. *Organometallics* **2007**, *26*, 4357−4360. (e) Jolley, K. E.; Zanotti-Gerosa, A.; Hancock, F.; Dyke, A.; Grainger, D. M.; Medlock, J. A.; Nedden, H. G.; Le Paih, J. J. M.; Roseblade, S. J.; Seger, A.; Sivakumar, V.; Prokes, I.; Morris, D. J.; Wills, M. Application of Tethered Ruthenium Catalysts to Asymmetric Hydrogenation of Ketones, and the Selective Hydrogenation of Aldehydes. *Adv. Synth. Catal.* **2012**, *354*, 2545−2555. (f) Diebolt, O.; Müller, C.; Vogt, D. ' On-Water" Rhodium-Catalysed Hydroformylation for the Production of Linear Alcohols. *Catal. Sci. Technol.* **2012**, *2*, 773−777. (g) Miyada, T.; Huang Kwan, E.; Yamashita, M. Synthesis, Structure, and Bonding Properties of Ruthenium Complexes Possessing a Boron-Based PBP Pincer Ligand and Their Application for Catalytic Hydrogenation. *Organometallics* **2014**, *33*, 6760−6770. (h) Bonomo, L.; Kermorvan, L.; Dupau, P. Ruthenium-Catalyzed Highly Chemoselective Hydrogenation of Aldehydes. *ChemCatChem* **2015**, *7*, 907−910. (i) Ngo, A. H.; Adams, M. J.; Do, L. H. Selective Acceptorless Dehydrogenation and Hydrogenation by Iridium Catalysts Enabling Facile Interconversion of Glucocorticoids. *Organometallics* **2014**, *33*, 6742−6745. (j) Mazza, S.; Scopelliti, R.; Hu, X. Chemoselective Hydrogenation and Transfer Hydrogenation of Aldehydes Catalyzed by Iron(II) PONOP Pincer Complexes. *Organometallics* **2015**, *34*, 1538−1545. (k) Tan, X.; Wang, G.; Zhu, Z.; Ren, C.; Zhou, J.; Lv, H.; Zhang, X.; Chung, L. W.; Zhang, L.; Zhang, X. Hydrogenation of Aldehydes Catalyzed by an Available Ruthenium Complex. *Org. Lett.* **2016**, *18*, 1518−1521. (l) Glatz, M.; Stöger, B.; Himmelbauer, D.; Veiros, L. F.; Kirchner, K. Chemoselective Hydrogenation of Aldehydes under Mild, Base-Free Conditions: Manganese Outperforms Rhenium. *ACS Catal.* **2018**, *8*, 4009−4016. (m) Cano, I.; Martinez-Prieto, L. M.; Vendier, L.; van Leeuwen, P. W. N. M. An Iridium-SPO Complex as Bifunctional Catalyst for the Highly Selective Hydrogenation of Aldehydes. *Catal. Sci. Technol.* **2018**, *8*, 221−228. (n) Christie, F.; Zanotti-Gerosa, A.; Grainger, D. Hydrogenation and Reductive Amination of Aldehydes using Triphos Ruthenium Catalysts. *ChemCatChem* **2018**, *10*, 1012−1018. (o) Casey, C. P.; Guan, H. Trimethylsilyl-Substituted Hydroxycyclopentadienyl Ruthenium Hydrides as Benchmarks to Probe Ligand and Metal Effects on the Reactivity of Shvo Type Complexes. *Organometallics* **2012**, *31*, 2631−2638. (p) Blum, Y.; Czarkie, D.; Rahamim, Y.; Shvo, Y. (Cyclopentadienone)ruthenium Carbonyl Complexes - A New Class of Homogeneous Hydrogenation Catalysts. *Organometallics* **1985**, *4*, 1459−1461. (q) Baldino, S.; Facchetti, S.; Zanotti-Gerosa, A.; Nedden, H. G.; Baratta, W. Transfer Hydrogenation and Hydrogenation of Commercial-Grade Aldehydes to Primary Alcohols Catalyzed by 2-(Aminomethyl)pyridine and Pincer Benzo[*h*]-quinoline Ruthenium Complexes. *ChemCatChem* **2016**, *8*, 2279−2288.
(19) Dupau, P.; Bonomo, L.; Kermorvan, L. Unexpected Role of Anionic Ligands in the Ruthenium-Catalyzed Base-Free Selective Hydrogenation of Aldehydes. *Angew. Chem., Int. Ed.* **2013**, *52*, 11347−11350.
(20) Albrecht, M. Cyclometalation Using d-Block Transition Metals: Fundamental Aspects and Recent Trends. *Chem. Rev.* **2010**, *110*, 576−623.
(21) (a) Rowland, R. S.; Taylor, R. Intermolecular Nonbonded Contact Distances in Organic Crystal Structures: Comparison with Distances Expected from van der Waals Radii. *J. Phys. Chem.* **1996**, *100*, 7384−7391. (b) Reedijk, J. Coordination Chemistry Beyond Werner: Interplay Between Hydrogen Bonding and Coordination. *Chem. Soc. Rev.* **2013**, *42*, 1776−1783.
(22) (a) Yang, X.; Hall, M. B. Mechanism of Water Splitting and Oxygen-Oxygen Bond Formation by a Mononuclear Ruthenium Complex. *J. Am. Chem. Soc.* **2010**, *132*, 120−130. (b) Li, J.; Shiota, Y.; Yoshizawa, K. Metal-Ligand Cooperation in H_2 Production and H_2O Decomposition on a Ru(II) PNN Complex: The Role of Ligand Dearomatization-Aromatization. *J. Am. Chem. Soc.* **2009**, *131*, 13584−13585.
(23) 2-Methyltetrahydrofuran is a green solvent: Aycock, D. F. Solvent Applications of 2-Methyltetrahydrofuran in Organometallic and Biphasic Reactions. *Org. Process Res. Dev.* **2007**, *11*, 156−159.
(24) (a) Lan, X.; Wang, T. Highly Selective Catalysts for the Hydrogenation of Unsaturated Aldehydes: A Review. *ACS Catal.* **2020**, *10*, 2764−2790. (b) Mäki-Arvela, P.; Hájek, J.; Salmi, T.; Murzin, D. Yu. Chemoselective Hydrogenation of Carbonyl Compounds over Heterogeneous Catalysts. *Appl. Catal., A* **2005**, *292*, 1−49.
(25) (a) Vogt, M.; Gargir, M.; Iron, M. A.; Diskin-Posner, Y.; Ben-David, Y.; Milstein, D. A New Mode of Activation of CO_2 by Metal-Ligand Cooperation with Reversible C-C and M-O Bond Formation at Ambient Temperature. *Chem. - Eur. J.* **2012**, *18*, 9194−9197. (b) Huff, C. A.; Kampf, J. W.; Sanford, M. S. Role of a Noninnocent Pincer Ligand in the Activation of CO_2 at (PNN)Ru(H)(CO). *Organometallics* **2012**, *31*, 4643−4645. (c) Montag, M.; Zhang, J.; Milstein, D. Aldehyde Binding Through Reversible C-C Coupling with the Pincer Ligand Upon Alcohol Dehydrogenation by a PNP-Ruthenium Catalyst. *J. Am. Chem. Soc.* **2012**, *134*, 10325−10328. (d) Huff, C. A.; Kampf, J. W.; Sanford, M. S. Reversible Carbon-Carbon Bond Formation between Carbonyl Compounds and a Ruthenium Pincer Complex. *Chem. Commun.* **2013**, *49*, 7147−7149. (e) Vogt, M.; Nerush, A.; Iron, M. A.; Leitus, G.; Diskin-Posner, Y.; Shimon, L. J. W.; Ben-David, Y.; Milstein, D. Activation of Nitriles by Metal Ligand Cooperation. Reversible Formation of Ketimido- and Enamido-Rhenium PNP Pincer Complexes and Relevance to Catalytic Design. *J. Am. Chem. Soc.* **2013**, *135*, 17004−17018.

https://doi.org/10.1021/acs.organomet.1c00109
Organometallics 2021, 40, 1314−1327

(26) (a) Ladipo, F. T.; Kooti, M.; Merola, J. S. Oxidative Addition of O-H Bonds to Iridium(I): Synthesis and Characterization of (Phenolato)- and (Carboxylato)iridium(III) Hydride Complexes. *Inorg. Chem.* **1993**, *32*, 1681−1688. (b) Ladipo, F. T.; Merola, J. S. Synthesis, Structural Characterization, and Reactivity of the (>2-Benzoato)iridium(III) Hydride Complex [*mer*-$(Me_3P)_3$ lr(>2-$O_2CC_6H_5$)(H)][PF_6]. *Inorg. Chem.* **1993**, *32*, 5201−5205.
(27) (a) Tondreau, A. M.; Michalczyk, R.; Boncella, J. M. Reversible 1,2-Addition of Water to Form a Nucleophilic Mn(I) Hydroxide Complex: A Thermodynamic and Reactivity Study. *Organometallics* **2017**, *36*, 4179−4183. (b) Nguyen, D. H.; Trivelli, X.; Capet, F.; Swesi, Y.; Favre-Réguillon, A.; Vanoye, L.; Dumeignil, F.; Gauvin, R. M. Deeper Mechanistic Insight into Ru Pincer-Mediated Acceptorless Dehydrogenative Coupling of Alcohols: Exchanges, Intermediates, and Deactivation Species. *ACS Catal.* **2018**, *8*, 4719−4734.
(28) (a) Bianchini, C.; Meli, A.; Peruzzini, M.; Vizza, F. Oxidation of Primary Alcohols to Carboxylic Acids Made Easy at Iridium. *J. Am. Chem. Soc.* **1990**, *112*, 6726−6728. (b) Yang, Z.; Luo, R.; Zhu, Z.; Yang, X.; Tang, W. Harnessing the Reactivity of Iridium Hydrides by Air: Iridium-Catalyzed Oxidation of Aldehydes to Acids in Water. *Organometallics* **2017**, *36*, 4095−4098.
(29) Gusev, D. G. Revised Mechanisms of the Catalytic Alcohol Dehydrogenation and Ester Reduction with the Milstein PNN Complex of Ruthenium. *Organometallics* **2020**, *39*, 258−270.
(30) Rueping, M.; Koenigs, R. M.; Borrmann, R.; Zoller, J.; Weirich, T. E.; Mayer, J. Size-Selective, Stabilizer-Free, Hydrogenolytic Synthesis of Iridium Nanoparticles Supported on Carbon Nanotubes. *Chem. Mater.* **2011**, *23*, 2008−2010.
(31) Frisch, M. J.; Trucks, G. W.; Schlegel, H. B.; Scuseria, G. E.; Robb, M. A.; Cheeseman, J. R.; Scalmani, G.; Barone, V.; Petersson, G. A.; Nakatsuji, H.; Li, X.; Caricato, M.; Marenich, A.; Bloino, J.; Janesko, B. G.; Gomperts, R.; Mennucci, B.; Hratchian, H. P.; Ortiz, J. V.; Izmaylov, A. F.; Sonnenberg, J. L.; Williams-Young, D.; Ding, F.; Lipparini, F.; Egidi, F.; Goings, J.; Peng, B.; Petrone, A.; Henderson, T.; Ranasinghe, D.; Zakrzewski, V. G.; Gao, J.; Rega, N.; Zheng, G.; Liang, W.; Hada, M.; Ehara, M.; Toyota, K.; Fukuda, R.; Hasegawa, J.; Ishida, M.; Nakajima, T.; Honda, Y.; Kitao, O.; Nakai, H.; Vreven, T.; Throssell, K.; Montgomery, J. A., Jr.; Peralta, J. E.; Ogliaro, F.; Bearpark, M.; Heyd, J. J.; Brothers, E.; Kudin, K. N.; Staroverov, V. N.; Keith, T.; Kobayashi, R.; Normand, J.; Raghavachari, K.; Rendell, A.; Burant, J. C.; Iyengar, S. S.; Tomasi, J.; Cossi, M.; Millam, J. M.; Klene, M.; Adamo, C.; Cammi, R.; Ochterski, J. W.; Martin, R. L.; Morokuma, K.; Farkas, O.; Foresman, J. B.; Fox, D. J. *Gaussian 09*, Revision E.01; Gaussian, Inc.: Wallingford, CT, 2016.
(32) (a) Becke, A. D. Density-Functional Thermochemistry. III. The Role of Exact Exchange. *J. Chem. Phys.* **1993**, *98*, 5648−5652. (b) Lee, C.; Yang, W.; Parr, R. G. Development of the Colle-Salvetti Correlation-Energy Formula into a Functional of the Electron Density. *Phys. Rev. B: Condens. Matter Mater. Phys.* **1988**, *37*, 785−789. (c) Miehlich, B.; Savin, A.; Stoll, H.; Preuss, H. Results Obtained with the Correlation Energy Density Functionals of Becke and Lee, Yang and Parr. *Chem. Phys. Lett.* **1989**, *157*, 200−206.
(33) Grimme, S.; Ehrlich, S.; Goerigk, L. Effect of the Damping Function in Dispersion Corrected Density Functional Theory. *J. Comput. Chem.* **2011**, *32*, 1456−1465.
(34) (a) Hehre, W. J.; Ditchfield, R.; Pople, J. A. Self-consistent Molecular Orbital Methods. XII. Further Extensions of Gaussian-Type Basis Sets for Use in Molecular Orbital Studies of Organic Molecules. *J. Chem. Phys.* **1972**, *56*, 2257−2261. (b) Hariharan, P. C.; Pople, J. A. The Influence of Polarization Functions on Molecular Orbital Hydrogenation Energies. *Theoret. Chim. Acta* **1973**, *28*, 213−222. (c) Francl, M. M.; Pietro, W. J.; Hehre, W. J.; Binkley, J. S.; Gordon, M. S.; DeFrees, D. J.; Pople, J. A. Self-Consistent Molecular Orbital Methods. XXIII. A Polarization-Type Basis Set for Second-Row Elements. *J. Chem. Phys.* **1982**, *77*, 3654−3665.
(35) Andrae, D.; Häußermann, U.; Dolg, M.; Stoll, H.; Preuss, H. Energy-adjusted *ab initio* Pseudopotentials for the Second and Third Row Transition Elements. *Theoret. Chim. Acta* **1990**, *77*, 123−141.
(36) Marenich, A. V.; Cramer, C. J.; Truhlar, D. G. Universal Solvation Model Based on Solute Electron Density and on a Continuum Model of the Solvent Defined by the Bulk Dielectric Constant and Atomic Surface Tensions. *J. Phys. Chem. B* **2009**, *113*, 6378−6396.
(37) Bruker *APEX2*; Bruker AXS, Inc.: Madison, WI, 2007.
(38) Bruker Advanced X-ray Solutions. *SAINT and SADABS Programs*; Bruker AXS Inc.: Madison, WI, 2004.
(39) Burla, M. C.; Camalli, M.; Carrozzini, B.; Cascarano, G. L.; Giacovazzo, C.; Polidori, G.; Spagna, R. SIR2002: the Program. *J. Appl. Crystallogr.* **2003**, *36*, 1103.
(40) Spek, A. L. Single-crystal Structure Validation with the Program *PLATON*. *J. Appl. Crystallogr.* **2003**, *36*, 7−13.
(41) van der Sluis, P.; Spek, A. L. BYPASS: An Effective Method for the Refinement of Crystal Structures Containing Disordered Solvent Regions. *Acta Crystallogr., Sect. A: Found. Crystallogr.* **1990**, *46*, 194−201.

https://doi.org/10.1021/acs.organomet.1c00109
Organometallics 2021, 40, 1314−1327